CHAPTER V
METAL ION ADSORPTION AND DESORPTION IN BATCH EXPERIMENTS

5.1 Adsorption studies

5.1.1 Effect of pH for adsorption

The solution pH affects the surface charge of the adsorbent and the degree of ionization of the speciation of the adsorbate and therefore affects the adsorption efficiency of the metal pollutants from wastewaters. Figure 5.1 demonstrates that the adsorption capacities of Cu and Pb increased with pH. The optimum pH for the adsorption of Cu(II) and Pb(II) (0.3 mmolL^{-1}) were about 5 which was slightly acidic. Figure 5.2 illustrates the relation between zeta potential and the pH of the solution and the results indicated that activated carbon surface had negative charge at pH higher than 2. In other words, the point of zero charge or PZC was less than 2. Hence, the activated carbon could be used as sorbent for positively charged contaminants such as heavy metal ions above this pH range. This was attributed to the fact that, at low pH (<3), the protonation of the active sites at carbon surface was enhanced and this refused the formation of links between metal ion and the active site. At moderate pH (3-6), linked H$^+$ was released from the active sites allowing more metal ions to be adsorbed to the vacant sites. Higher pH values (>6) generally decrease the electrostatic repulsion between cations and also the positively charged surface, which promotes higher adsorption capacity. Therefore maximum adsorption often occurs at high pH level. On the other hand, an increase in pH meant a lower quantity of protons, which caused a decrease in the competition between proton and heavy metal ion. However, metal precipitation took place at high pH and this would interfere with the adsorption characteristics. Hence, an increase in the sorption capacity (or removal efficiency) could be observed. Therefore it is important that a suitable pH for the adsorption be identified. To ensure no interference from metal precipitation, subsequent experiments were carried out at pH less than or equal to 5 (see Figure 5.2). In practice, metal precipitation is generally not a stabilized form of heavy metals as the precipitates can be very small in size, and upon the neutralization of the effluent from the wastewater treatment plant, the solubility of the metals increases resulting in a re-contamination of the waste outlet stream.

5.1.2 Adsorption kinetics

Figure 5.3(a) and (b) demonstrate the time profile of the adsorptions of both Cu(II) and Pb(II) onto the activated carbon at different initial concentrations (0.1-10mM). Generally, the adsorption capacity increased with time until equilibrium was attained between the amounts of metals adsorbed on the activated carbon and the remaining in the solution. The adsorption took place more rapidly at initial stages and gradually slowed down. This behavior is quite common due to the saturation of the available adsorption sites (Yardim et al., 2003). The time to reach equilibrium varied with the initial concentration, i.e. the solution with a higher initial concentration required a slightly longer time than the solution with a lower initial concentration, however, experiments revealed that equilibrium was reached within 45 min for all cases investigated in this work. Figure 5.3(a) and (b) demonstrate that the kinetic curves were generally smooth and continuous, and the saturation could be expected to occur indicating a monolayer adsorption of metal ion on the carbon surface.

In order to characterize the kinetic behavior of a reaction, it was common to determine how the rate of reaction varied as the reaction proceeded. Lagergren's first order kinetic equation has been most widely used to describe the solute adsorption on various adsorbents (Ho, 2003), and this can be expressed as (Lagergren, 1898):

$$log(q_e - q) = \log q_e - \frac{k_1}{2.303}t \tag{5.1}$$

where q_e and q are the amounts of adsorbed metal on the sorbent at the equilibrium and at time t, respectively (mg g^{-1}), and k_1 is the rate constant of first-order sorption (min^{-1}). Another most widely used kinetic expression is the pseudo second-order rate expression derived by Ho and McKay (2003) where sorption capacity was assumed to be proportional to the number of active sites occupied on the sorbent:

$$\frac{t}{q} = \frac{1}{k_2 q_e^2} + \frac{1}{q_e}t \tag{5.2}$$

where k_2 is the pseudo second-order rate constant with a unit of g mg^{-1} min^{-1}.

The experimental data were fitted with these two kinetics models where the kinetic parameters such as rate constants and equilibrium adsorption capacities of adsorption for Cu(II) and Pb(II) are summarized in Table 5.1. However, the results illustrate that a linear relationship between $log(q_e-q)$ and t could not be obtained indicating that the first order

Lagergren rate kinetics was not appropriate to describe the adsorption. The data seemed to fit much better with the pseudo second-order kinetics where kinetic parameters, q_e and k_2, are summarized in Table 5.1.

Table 5.1 also shows that the equilibrium sorption capacity, q_e, of Cu(II) and Pb(II) increased from 0.0194 to 0.479 mmol g^{-1} and 0.177 to 0.551 mmol g^{-1}, respectively, as the initial concentration varied from 0.1 to 10 mmol l^{-1}. A comparison of the experimental sorption capacities and calculated values obtained from Eqs. (5.1) and (5.2) shows that the calculated q_e for the adsorption of Cu at initial concentration of 0.3 mmol l^{-1} from the pseudo-first-order kinetic model (= 0.003 mmol g^{-1}) differed largely from experimental q_e of 0.0563 mmol g^{-1}. On the other hand, the calculated q_e of 0.0564 mmol g^{-1} from the second order model was significantly closer to the experimental q_e. Extremely good agreements between the results and the model were obtained as illustrated by the very high R^2 for the whole range of initial metal concentrations which, by and large, confirmed the applicability of the pseudo-second-order kinetics. Hence, it was concluded at this point that the adsorption here could be better represented by the pseudo second-order rate kinetics.

In addition, the results indicated that an increase in initial metal concentration increased the rate constant (k_2). High k_2 suggested that the metal could be rapidly sequestered by the activated carbon functional groups, resulting in the system quickly reaching equilibrium as reported earlier. This was because an increase in initial metal concentration enhanced the concentration gradient of metal ion between aqueous and solid phases. Consequently, the mass transfer of adsorbate into adsorbent increased. This finding supported the assumption of the pseudo second order model that the sorption process was due to chemisorption (Ho, 2003). In this case, chemical sorption could have occurred by the interaction between polar functional groups on the adsorbent surface and the metals.

5.1.3 Adsorption isotherm

The adsorption isotherms of Cu(II) and Pb(II) ions on activated carbon are illustrated in Figure 5.4. Adsorption isotherm is the relationship between adsorption capacity and concentration of the remaining adsorbate at constant temperature. Generally there are two mathematical expressions used to describe the isotherm of the adsorption; (i) Langmuir and (ii) Fruendlich equations. Langmuir's isotherm (Langmuir, 1916; 1918) is of the form

$$\frac{C_e}{q_e} = \frac{1}{q_m b} + (\frac{1}{q_m})C_e \tag{5.3}$$

Figure 5.4 illustrates the plots of Cu(II) and Pb(II) ions which shows that a straight line could be well observed between C_e/q_e and C_e. This indicated that the experimental data followed Langmuir's isotherm. The maximum adsorption capacity (q_m) and the Langmuir constant (b) were calculated from this plot and the results are summarized in Table 5.2. The Langmuir parameters, i.e. q_m increased with temperature. High temperatures increased the kinetic energy of the metal and, hence, enhanced the mobility of the metal ions. This led to a higher chance of the metal being adsorbed onto the adsorbent and an increase in its adsorption capacity.

The Freundlich isotherm (Freundlich, 1906) is given by:

$$q_e = K_F C_e^{1/n} \tag{5.4}$$

where K_F and n are constants of Freundlich isotherm incorporating adsorption capacity (mmol g^{-1}) and intensity, while C_e and q_e are the remaining concentration of adsorbate after equilibrium (mmol g^{-1}) and the amount adsorbed at equilibrium (mmol g^{-1}), respectively. The Freundlich constants, i.e., $1/n$ and K_f, were calculated from the slope and interception of the Freundlich plots, respectively, and the results are summarized in Table 5.2.

As both the Langmuir and Freundlich models could explain the adsorption. This suggested that the adsorption of Cu(II) and Pb(II) was potentially monolayer (Feng et al., 2004). The values of $1/n$ of less than 1 confirmed a favorable adsorption onto microporous adsorbent (Faur-Brasquet et al., 2002). A comparison between maximum adsorption capacities (q_m) between the two metal ions illustrated that Cu(II) and Pb(II) had maximum adsorption capacities of 0.45 and 0.53 mmol g^{-1}, respectively. It was indicated that activated carbon had higher maximum adsorption capacity for Pb(II). Moreover, Pb(II) adsorption was found to have a higher b value than Cu(II) indicating that this activated carbon had higher affinity for Pb(II) than Cu(II).

5.1.4 Effect of temperature on metal uptake

The adsorptions of Cu(II) and Pb(II) onto activated carbon were favored at higher temperatures as shown in Table 5.2. This may indicate that adsorption of Cu(II) and Pb(II) onto activated carbon are of chemical nature. An increase in the temperature from 25 to 60°C led to an increase in the adsorption capacity from 0.45 to 0.85 mmol g^{-1} for Cu(II) and 0.55 to 0.89 mmol g^{-1} for Pb(II), respectively. Adsorption capacities of the activated carbon increased

rapidly first with an increase in initial concentrations of Cu(II) and Pb(II) and reached a saturation values of around 10 mmol l^{-1} for Cu(II) and Pb(II) as show in Figure 5.5(a) and 5.5(b). Greater removal levels for Cu(II) and Pb(II) were observed in higher temperature range. This was due to the increasing tendency of adsorbate ions to move from the solution to the interface with increasing temperature. The increase of the equilibrium uptake at increased temperature indicated that the adsorption of Cu(II) and Pb(II) ions to activated carbon was endothermic.

5.1.5 Enthalpy of adsorption

The apparent heat or net enthalpy of adsorption, ΔH, is related to the Langmuir constant, b, as presented in Eq. (5.5) (Faust and Aly, 1987):

$$\ln b = \ln b' - \frac{\Delta H}{RT} \qquad (5.5)$$

where b' is a constant, R the gas constant (8.314 J mol^{-1} K^{-1}), and T the temperature in Kelvin. The slope of the plot of $\ln b$ versus $1/T$ of Cu(II) and Pb(II) in Figure 5.6(a) and (b) represent - $\Delta H/R$ which allows the calculation of ΔH. The value ΔH of Cu(II) and Pb(II) were 43.26 and 58.77 kJ mol^{-1}, respectively. This suggested that the chemical bond between the activated carbon surface and the metal ions could not be easily desorbed by physical means such as simply shaking or heating.

Table 5.3 reveals that for a particular adsorbed metal ion, q_e increased with temperature. The second-order rate constant is expressed as a function of temperature by the following Arrhenius type relationship:

$$\ln k = \ln A_0 - \frac{E_a}{RT} \qquad (5.6)$$

where A_o is the temperature independent factor called "frequency factor" (g $mmol^{-1}$ min^{-1}), k the rate constant of adsorption (min^{-1}), E_a the activation energy for adsorption (kJ mol^{-1}), R the gas constant (8.314 J mol^{-1} K^{-1}), and T the temperature in Kelvin.

A linear relationship was obtained between $\ln k_2$ and $1/T$. The values of E_a/R was calculated from slope of the $\ln k_2$ versus $1/T$ plot (see Figure 5.7) and, in this case, it was found to be 28.05 kJ mol^{-1} for Cu(II) and 40.05 kJ mol^{-1} for Pb(II), respectively. The magnitude of activation energy may give an idea about the type of adsorption. Two main types of adsorption: physical and chemical are possible. In physical adsorption the reaction is

easily reversible, equilibrium is rapidly attained and its energy requirements are small. The activation energy for physical adsorption is usually not more than 8 kJ mol^{-1}, because the forces involved in physical adsorption are usually weak, and so the activation energy is of the same magnitude as the heat of chemical reactions. However, chemical adsorption is specific and involves forces much stronger than physical adsorption (Aksu, 2001). The activation energies for adsorption was found to be between 0 and 50 kJ mol^{-1} (on the average 18 kJ mol^{-1}), leading to a positive temperature dependence of adsorption rate (Hulscher and Cornelissen, 1996). The value E_a in the present study indicated that the chemical sorption process was mainly involved in the reaction with strong interactions between sorbent and sorbate (Ho et al., 2001). The positive values of E_a and ΔH indicated the presence of an energy barrier in the adsorption process, or in other words, the adsorption was endothermic (Ozcan and Ozcan, 2004).

5.1.6 Relationship between functional groups and heavy metals adsorption

The functional groups on the surface of activated carbon as analyzed by FT-IR demonstrated the existence of carboxyl, hydroxyl, and amine groups which are mostly negatively charged. The FT-IR transmission spectra in the range of 450–4000 cm^{-1} for the original activated carbon and the activated carbon laden with Cu(II), and Pb(II) are shown Figure 5.8(a), (b) and (c) and the FT-IR spectroscopic characteristics are shown in Table 5.4. Figure 5.8(a), (b) and (c) demonstrate that, after the adsorption, there seemed to be shifts and intensity decreases in wave number of dominant peaks. These clear band shifts and intensity decreases could be observed at 3390.59, 1693.14, 1200.85, 1088.49, 823.21 and 500.36 cm^{-1} for Cu(II)-laden activated carbon, and at 3390.59, 1693.14, 1200.85, 517.88 and 500.36 cm^{-1} for Pb(II)-laden activated carbon. These shifts indicated that there were binding processes taking place on the surface of activated carbon (Pavasant et al., 2003). Summary of the functional groups involved in the adsorption were as follows: broad bands at 3390.59 cm^{-1} representing bonded –OH groups, 2943.07–2866.90 cm^{-1} the aliphatic C–H group, 2065.57-1693.14 cm^{-1} the C=O stretch, 1590.93 cm^{-1} the secondary amine group, 1200.85 cm^{-1} the C-O stretch, 1088.49 cm^{-1} the P–O symmetrical vibration in a chain of P–O–P (polyphosphate) which formed in the samples carbonized in the presence of phosphoric acid, and the peaks at 828.21 cm^{-1} assigned to -CN stretching, 517.88-500.36 cm^{-1} C–C group in alkane. The spectral analysis before and after metal adsorption indicated that –OH groups,

C=O stretching, secondary amine group and symmetric bending of CH_3 were both involved in Cu(II) and Pb(II) adsorption. These functional groups could act as chemical binding agents where carboxyl, hydroxyl, and amine groups could dissociate giving negative charged active surface. That meant that these functional groups could attract the positive charge objects such as heavy metal ions (Volesky, 1990). It was worth noting that the functional groups for Cu(II) were also available for the Pb(II) adsorption.

5.2 Desorption studies

5.2.1 Type of solvent for desorption
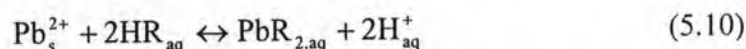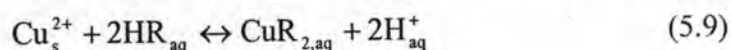
Single component system

From the process point of view, the desorption or the release of bound metals does not only result in the recovery of the metal, but it also does help regenerate the activated carbon, enabling further reuse of the activated carbon. From adsorption experiments, the metal loaded activated carbon was obtained from batch experiments with 10 mmol L^{-1} of metal solution which gave the adsorption capacities of 0.45 and 0.55 mmol g^{-1} of Cu(II) and Pb(II), respectively. In desorption experiments, the amount of metal loaded in activated carbon were analyzed by digestion the metal loaded activated carbon which demonstrated the actual amount of metal in activated carbon. The digestion experiment illustrated that the amount of Cu(II) and Pb(II) from the metal loaded activated carbon were 0.47 and 0.56 mmol g^{-1}, respectively. These were higher than the values obtained from adsorption experiments. The desorption agents were of the acidic type to facilitate the metal dissolution, these mediums include phosphoric, sulfuric and citric acid solutions. The amount of metal released is calculated from:

$$q_{Ext} = \frac{(q_{ad} \times W) - (C_{Ext} \times V)}{W} \qquad (5.7)$$

where q_{ext} and q_{ad} are extraction capacity and adsorption capacity before extraction (mmol g^{-1}) C_{Ext} the concentration of metal extracted into the solvent (mmol l^{-1}), W the adsorbent dosage (g) and V the solution volume (L). The extraction efficiency is calculated from:
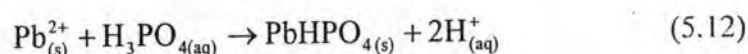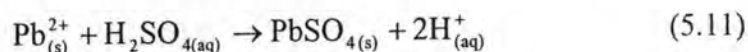
$$Extraction\ efficiency = \frac{C_{Ext} \times V}{q_{ad} \times W} \times 100\% \qquad (5.8)$$

The data obtained from the desorption of Cu(II) and Pb(II) using various desorbing agents are shown in Table 5.5. Figure 5.9 which demonstrate the effect of the type of solvent for desorption Cu(II) and Pb(II). The efficiency of the elution solutions could be ordered from high to low as: citric acid > sulfuric acid > phosphoric acid for Cu(II); and citric acid > phosphoric acid > sulfuric acid for Pb(II). Citric acid was found to be most efficient with desorption efficiency of 92.14% and 95.80% for Pb(II) and Cu(II), respectively. This could be because citric acid could form metal-citrate complex where proton could replace metal ions loaded on the activated carbon surface (Lee et al., 2005), similar results were reported by Martell and Smith (1977) and Qin et al. (2004). The following mechanism was proposed:

$$Cu_s^{2+} + 2HR_{aq} \leftrightarrow CuR_{2,aq} + 2H_{aq}^+ \qquad (5.9)$$

$$Pb_s^{2+} + 2HR_{aq} \leftrightarrow PbR_{2,aq} + 2H_{aq}^+ \qquad (5.10)$$

where HR represents the extractant and the subscripts 's' and 'aq' refer to the solid and aqueous phases.

The solubility of metals in different acid solutions depends strongly with the complex affinity of the metal ions (Terry and Monhemius, 1983; Souza et al., 2007). For instance, sulfuric and phosphoric acids were not effective desorbing agents for Pb(II) due to the formation of lead sulphate precipitate ($PbSO_4$) (Sampedro et al.,1995) and insoluble lead phosphate ($PbHPO_4$) (Niragu, 1972; Mouflih et al., 2004), respectively:

$$Pb_{(s)}^{2+} + H_2SO_{4(aq)} \rightarrow PbSO_{4(s)} + 2H_{(aq)}^+ \qquad (5.11)$$

$$Pb_{(s)}^{2+} + H_3PO_{4(aq)} \rightarrow PbHPO_{4(s)} + 2H_{(aq)}^+ \qquad (5.12)$$

Binary component system

Cu-Pb was arbitrarily selected as a modeled binary mixture where the ultimate goal was to separate the two metal ions to evaluate for the potential in metal recovery. From the binary adsorption in column experiments, Cu(II) and Pb(II) at equimolar concentration of 0.15 mmol L^{-1} (a total of 0.3 mmol L^{-1}) were studied. The amounts of Pb(Cu-Pb) and Cu(Cu-Pb) adsorbed onto one gram of activated carbon were 0.046 and 0.033 mmol, respectively. This values were calculated from the breakthrough curves of Pb(Cu-Pb) and Cu(Cu-Pb) at C/Co ratios higher than 0.1 and lower than 0.95, and not the exact the value of metal adsorption. Hence, digestion experiment was carried out to determine the amount of metal

adsorbed in activated carbon. Digestion of activated carbon samples showed that the amounts of Pb(Cu-Pb) and Cu(Cu-Pb) adsorbed onto activated carbon were 0.036 and 0.049 mmol g^{-1}, respectively. This loaded activated carbon was then eluted with the three acid solutions in a similar manner to that of single component systems. From the single component desorption, citric acid was found to have strong affinity for Cu(II) than Pb(II). This was not desirable for the multiple component adsorption systems particularly when the recovery of each metal is required as both metals would be leached out in the solution and no separation was achieved. On the other hand, the separation of the two metals could be possible with the desorption conditions that provided rather different desorption efficiency for the two metals. The single desorption experiment as described above suggested that phosphoric acid and sulfuric acid could facilitate this recovery process if proper desorption conditions were applied. Experiments were then carried out with the two acids and the results were compared which was in the favor of using sulfuric acid rather than phosphoric acid. This was evidenced in Figure 5.10 which illustrates that only sulfuric acid could provide reasonably high recovery of Cu(II) (69.35%), whilst at the same time, maintained the recovery of Pb(II) at the lowest possible level (0.61%). In fact, although sulfuric acid might not be as good as citric acid in leaching Cu(II) from the activated carbon, the desorption of Cu(II) with sulfuric acid was relatively a fast process. This was also observed from the work of Jandoûa et al. (2000).

A desorption ratio was proposed as an indicator for the effectiveness in the separation of the two metals, and is defined as the ratio between the amount of one species of metal released and the total amount of both species released from the activated carbon (Eq. (5.13).

$$\text{Desorption ratio of metal } i = \frac{\text{Concentration of metal } i}{\text{Concentration of metal } i + \text{Concentration of metal } j} \quad (5.13)$$
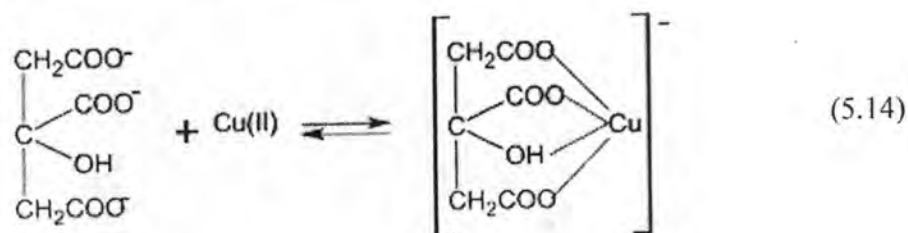
Table 5.6 illustrates the level of desorption ratio for Cu(II) from the binary component system. Sulfuric acid provided the highest Cu desorption ratio (high quantity of Cu(II) being leached out and low Pb(II)). In the comparison of the desorption efficiency of Cu(II) and Pb(II) in binary component systems, it was expected that the effectiveness of sulfuric acid on the extract of Cu(II) was better than that of Pb(II). This could be described using the concept of the stability of the metal-ligand system which is generally used to analyze complexation

data at specific pH where a more stable solution exhibits a higher stability constant. Jensen (2002) reported that the stability constant of sulfuric acid with Cu(II) was higher than Pb(II) (log $K_{Cu\text{-}sulphate}$ = 17.19, log $K_{Pb\text{-}sulphate}$ = 13.2). Therefore Cu(Cu-Pb) had a higher potential in being extracted by sulfuric acid than Pb(Cu-Pb). It could also be that the adsorption of Pb(Cu-Pb) was stronger than the adsorption of Cu(Cu-Pb) on the activated carbon and therefore the desorption could see a higher release of Cu(Cu-Pb) than that of Pb(Cu-Pb). In fact, the release of Pb(Cu-Pb) was quite small and with all conditions examined in this work, this Pb desorption efficiency was not greater than 1%. Hence, this desorption efficiency of Pb for the following discussion will not be mentioned if stated otherwise.

5.2.2 Effect of solvent concentration

Single component system

Figure 5.11 shows the percentage of desorption of each element individually using citric acids at different concentrations. It was found that the extraction efficiency increased with increasing solvent concentration. A similar phenomenon was also observed by Veeken and Hamelers (1999) who used citric acid to extract heavy metals from sewage sludge. As solvent concentration increased, the number of organic ligands available for complexing with metal ions and proton for replacing also increased (lower pH), which would then increase the extraction efficiency (Qin et al., 2004). The mechanism for the formation of a Cu(II)–citrate complex is suggested below (Eq. 5.14):

$$\begin{array}{c}
CH_2COO^- \\
\ \ |\ \ \diagdown COO^- \\
C \\
\ \ |\ \ \diagup OH \\
CH_2COO^-
\end{array}
+ Cu(II) \ \rightleftharpoons \
\left[\begin{array}{c}
CH_2COO \diagdown \\
\ \ |\ \ \diagdown COO \diagdown \\
C \qquad\qquad Cu \\
\ \ |\ \ \diagup OH \diagup \\
CH_2COO \diagup
\end{array}\right]^- \qquad (5.14)$$

In the presence of 1 N citric acid, the recovery efficiencies of Cu(II) and Pb(II) were 95.80 and 92.14%, respectively. With a further increase in the citric acid concentration from 1 to 3 N, the recovery efficiency for both metals remained relatively constant (94.45 at 1N VS 95.37% at 3N for Cu(II), and 91.78 at 1N VS 91.80% at 3N for Pb(II)) in comparison to solvent with lower citric acid concentration, i.e. 0.5–1 N. Within the high acid concentration range, there should be adequate acid for the desorption process, unlike at low concentration

range, where there might not have enough citric acid for the extraction. Therefore, the recovery of the metal in subsequent experiments was carried out using 1 N citric acid.

Binary component system

Figure 5.12 illustrates the desorption efficiencies of both Cu(II) and Pb(II) at various sulfuric acid concentrations. The results indicated that the optimal condition for desorption was obtained from the acid at 1 N which provided almost 69% recovery of Cu from the binary component. The recovery efficiency for Cu(Cu-Pb) increased with increasing concentration of desorbing agent from 0.5 to 1 N (from 47.29 to 69.35%). At concentration above 1 N, similar to the single component system, the recovery efficiency for Cu(Cu-Pb) remained, by and large, at constant level, or in fact, very slightly decreased, i.e. from 69.35 to 68.65 for 2 N sulfuric acid, and also decreased to 68.64 and 67.73% at 2.5 and 3 N, respectively. It is noted here that the desorbing agent concentration of 1 N provided the best desorption efficiency.

5.2.3 Effect of contact time

Single component system

In desorption processes, heavy metals loaded on activated carbon are pushed back into the fresh desorbing agent. The concentration of heavy metals in the desorbing agent generally increases with time, whereas the amount of heavy metals on the activated carbon decreases. This is exactly the reverse of the adsorption process where Figures 5.13-5.14 illustrates the desorption time profiles and extraction efficiencies of Cu(II) and Pb(II) in the single component systems by 1 N citric acid. It was quite clear that the amount of released metal ions increased with increasing contacting time for both Cu(II) and Pb(II) extractions. The equilibrium state was achieved within 60 min under the desorption conditions used in this work.

Desorption kinetics of Cu(II) and Pb(II) from loaded activated carbon were studied by using experiment condition of citric acid concentration equal to 1 N. This condition gave almost 100% recoveries of Cu(II) and Pb(II) (Figure 5.13). For the rate of desorption to follow the first-order kinetics, the following equation must be fulfilled:

$$-\frac{dq}{dt} = k_{d,1}(q - q_e) \tag{5.15}$$

where q_e and q are the amount of adsorbate on the adsorbent at the equilibrium and at time t, respectively (mmolg^{-1}), and $k_{d,1}$ is the rate constant of first-order desorption (min^{-1}). After integrating and applying boundary condition, $t=0$ - $t=t$ and $q=q_0$ - $q=q$; Eq. (5.15) becomes

$$\log(q - q_e) = \log(q_0 - q_e) - k_{d,1}t \qquad (5.16)$$

On the other hand, if the desorption is to follow the second order kinetics, the following expression should be valid:

$$-\frac{dq}{dt} = k_{d,2}(q - q_e)^2 \qquad (5.17)$$

where $k_{d,2}$ are the second-order rate constant with a unit of g mmol^{-1} min^{-1}. After integrating and applying boundary condition, $t=0$ - $t=t$ and $q=q_0$ - $q=q$; Eq. (5.15) becomes

$$\frac{1}{(q - q_e)} - \frac{1}{(q_0 - q_e)} = k_{d,2}t \qquad (5.18)$$

The curve fitting provided the results as indicated in Table 5.7 which suggested that the second order kinetics were more accurate where, at 25°C, the rate constant of Cu(II) and Pb(II) desorptions were 0.58 and 0.33 g mmol^{-1} min^{-1}. The amount of metal ions at equilibrium state was 4.36×10^{-2} and 1.03×10^{-1} mmol g^{-1}. The quantities of Cu(II) and Pb(II) equilibrium concentration in solution were always lower than the original concentration before the sorption. This indicates that some reactions involved in the sorption processes may be irreversible or very slowly reversible. Comparing the $k_{d,2}$ values in (Table 5.7) indicates that the affinity of Cu(II) to the sorbents was greater than Pb(II).

Binary component system

Figures 5.15-5.16 demonstrate the desorption kinetics of Cu(Cu-Pb) with 1N sulfuric acid. It was quite clear that the amount of metal ions remaining in the activated carbon decreased with increasing contacting time for Cu(II) extraction and reached equilibrium in 60 min. The experimental data were fitted with these two kinetic models where the kinetic parameters such as rate constants and equilibrium desorption capacities for Cu(Cu-Pb) are summarized in Table 5.7. However, the results demonstrate that the first order Lagergren rate kinetics was not appropriate to describe the desorption. The data seemed to fit much better with the second-order kinetics.

5.2.4 Effect of temperature

Single component system

Desorption of Cu(II) and Pb(II) from loaded activated carbon was examined with 1 N citric acid. The effect of desorption temperature was investigated by performing experiments at different desorption temperatures: 25, 50, and 75 °C, and the results are presented in Table 5.7 and Figures 5.13-5.14. The desorption efficiency of the metals increased with an increase in temperature. For instance, at 25°C, 87.86% of Cu(II) and 76.62% of Pb(II) could be leached, and these were increased to 90.07% of Cu(II) and 81.81% of Pb(II) at 50°C. Further increase in temperature to 75°C saw an increase in the recovery of Cu(II) and Pb(II) to 95.80 and 92.14%, respectively. An increase in the desorption temperature enhanced the desorption efficiency resulting in a lesser quantity of metal ion remaining on the activated carbon. The increase in desorption efficiency could be due to thermodynamic equilibria where metal solubilities in acid solution increased with temperature (Nowack, 2003). Kinetic examinations showed that desorption rates of Cu(II) and Pb(II) significantly increased with increasing temperature. This was because an increase in temperature desorption enhanced the mobility gradient of metal ion between aqueous and solid phases.

Binary component system

The effect of temperature on the desorption efficiency was studied using 1 N sulfuric acid and the desorption time of 60 min. The results as presented in Figures 5.15-5.16 indicated that an increase in the desorption temperature enhanced the desorption efficiency of Cu(II) from binary component, although not in a great extent. For instance, the desorption efficiency of Cu(II) from binary component was 59.03% at 25°C, and this became 65.89%, at 50°C, and 69.35% at 75°C.

5.3 Properties of activated carbon after desorption

5.3.1 Fourier Transform Infared (FT-IR)

Tables 5.8-5.10 shows FT-IR spectra of the original activated carbon, metal-adsorption and after being desorbed by acid solvent extraction. Figure 5.17 (a), (b) and (c) demonstrates that there seemed to be shifts and intensity decreases in wave number of dominant peaks in the original activated carbon after the adsorption and also after the

desorption of Cu. This indicated changes in the structure of the activated carbon along the adsorption/desorption process. Figures 5.18-5.19 also present the same results with Pb(II) and the binary mixture of Cu(II) and Pb(II), respectively. These clear band shifts and intensity decreases could be observed at 3433.66 (–OH groups), 1707.48 (C=O stretch) and 1601.82 cm^{-1} (the secondary amine group) for Cu(II)-desorption, and at 3429.48 (–OH groups), 1706.16 (C=O stretch), 1053.21 (P–O symmetrical), 825.44 (-CN stretching), and 575.16-535.93 cm^{-1} (C–C group in alkane) for Pb(II)-desorption, and also intensity decreases to 3427.89 (–OH groups), 1593.86 (the secondary amine group) and 594.78 (C–C group in alkane) cm^{-1} for the binary-desorption. These implied a reduction in the availability of the following functional groups: broad bands at 3390.59 cm^{-1} representing bonded –OH groups, 1693.14 cm^{-1} the C=O stretch, 1590.93 cm^{-1} the secondary amine group, 1200.85 cm^{-1} the C-O stretch, 1088.49 cm^{-1} the P–O symmetrical, and the peaks at 828.21 cm^{-1} assigned to -CN stretching, 517.88-500.36 cm^{-1} C–C group in alkane. In other words, the newly generated activated carbon had the –OH group at 3390.59 cm^{-1}, this was shifted to 3429.33 cm^{-1} after the adsorption of Cu(II) in the Cu ion solution. After the desorption, the shift occurred again and this moved the –OH group to 3433.66 cm^{-1}. The same thing occurred with the Pb(II) single component (Figure 5.18 (a), (b) and (c)) and the binary Cu-Pb component systems (Figure 5.19 (a), (b) and (c)). Summaries of the potential functional group involved in the adsorption/desorption of Cu(II), Pb(II) and the binary mixture of the two metal ions are provided in Tables 5.8-5.10. This illustrates that there were differences in the target functional groups for each metal on the surface of activated carbon. It can also be realized that the structure of the activated carbon changed every time adsorption and desorption occurred. This indicated the instability of the activated carbon product obtained from this work.

5.3.2 X-ray fluorescence (XRF)

After solvent extraction, the intensity of the fluorescent radiation of Cu-desorption, Pb-desorption and binary-desorption in the samples of activated carbon were measured by X-ray fluorescence (XRF). This was to check whether the metal(s) was really desorbed from the activated carbon structure. Figure 5.20 (a) and (b) illustrates the XRF patterns of activated carbon with Cu-adsorbed and after the Cu-desorption with citric acid. This demonstrated that Cu disappeared from the activated carbon after the desorption. Citric acid solution could achieve 86% extraction of Cu(II) from loaded-activated carbon. Similarly, Figure 5.21 (a) and

(b) illustrates that 84.32% of Pb was actually leached out by citric acid as the Pb peak disappeared after the desorption with citric acid. For the binary mixture, Figure 5.22 (a) and (b) clearly demonstrates that only Cu(II) could be extracted by sulfuric acid as the XRF-peak for Cu disappeared after the extraction process whilst the peak for Pb remained in the carbon structure. In this case, the amount of extracted Cu(II) was the highest at 65.79% when compared with the initial concentration in the loaded activated carbon. At this condition, Pb(II) could only be extracted at 0.73%.

5.3.3 Iodine and methylene blue numbers

To estimate the applicability of the activated carbon product as an adsorbent, adsorption tests were performed using iodine and methylene blue solutions as adsorbate. The value of iodine and methylene blue numbers after desorption were 473.23 and 285.46 mg g^{-1}, respectively. These were quite low when compared to the original values using newly generated activated carbon of 1,226 and 425.5 mg g^{-1} for iodine and methylene blue numbers. It could be that, after desorption, some components, e.g. metal, and desorbing agent remained deposited in the pore, reducing the porous structure of activated carbon. Moreover, desorbing agent could also destroy the functional groups of activated carbon, resulting in changes of activated carbon structure.

5.3.4 Specific surface area

BET surface area obtained after desorption (651.3 m^2 g^{-1}) was a lower than original activated carbon (1,354 m^2 g^{-1}). This may be explained by the fact that desorbing agent also reacted the surface of the activated carbon resulting in a widening of pore structure. Therefore this increased the fraction of macro- and mesopore in the carbon structure. In addition, the collapse of micropore walls could also take place when the surface reaction with acid occurred.

5.4 Concluding remarks

Table 5.11 shows a summary of various adsorbents previously studied for Cu(II) and Pb(II) removal. It can be seen that the adsorption capacity of the activated carbon from eucalyptus bark was among the highest available which makes the adsorbents viable for metal removal in actual wastewater facilities. The eucalyptus bark (in this work) could be effectively converted to activated carbon with relatively high levels of BET surface area when

compared to other types of raw materials. The difference could be due to the different nature of raw materials (Chen et al., 2003), and this led to a different formation of pore structure in the final activated carbon product. The results indicate the potential application of such activated carbon in wastewater treatment facilities.

The desorption study illustrates that the recovery of each metal could be achieved with a proper selection of desorbing agent, and in this case, sulfuric acid was the most suitable medium where only Cu(II) was leached out from the carbon whilst maintaining Pb(II) in the carbon surface. This potentially allowed the recovery of each individual metal from the binary mixture of metals solution. However, the desorption study also demonstrated that the activated carbon product produced from eucalyptus bark lost its properties quite significantly after the adsorption. This loss of adsorption capacity by activated carbon after each cycle could be associated with interactions between the desorbing agent and the functional groups or active sites on the activated carbon which resulted in, e.g. structural damage and blockage of binding sites (Zhou et al., 1998). Nevertheless the surface area of the activated carbon after the desorption was still in the middle range among the activated carbon generated from various sources of agricultural raw materials as stated in Table 5.11.

Table 5.1 Kinetic parameters of pseudo first and second-order models for single component adsorptions of Cu(II) and Pb(II) at 25^0C

Heavy metals	Initial concentration (mmol L^{-1})	$q_{e,exp}$ (mmol g^{-1})	Pseudo-first order			Pseudo-second order		
			k_1 (min^{-1})	$q_{e,cal}$ (mmol g^{-1})	R^2	k_2 (g mmol^{-1} min^{-1})	$q_{e,cal}$ (mmol g^{-1})	R^2
Cu(II)	0.1	1.97×10^{-2}	4.05	1.92×10^{-2}	0.9976	3.22×10^{-4}	1.94×10^{-2}	0.9997
	0.2	3.91×10^{-2}	3.22	3.86×10^{-2}	0.9995	5.87×10^{-4}	3.90×10^{-2}	1.0000
	0.3	5.63×10^{-2}	3.13	5.51×10^{-2}	0.9971	8.00×10^{-4}	5.64×10^{-2}	1.0000
	0.4	7.99×10^{-2}	2.66	7.84×10^{-2}	0.9962	4.62×10^{-3}	7.95×10^{-2}	0.9998
	0.5	9.11×10^{-2}	2.05	9.16×10^{-2}	0.9882	5.01×10^{-3}	9.36×10^{-2}	0.9999
	1.0	1.73×10^{-1}	2.09	1.61×10^{-1}	0.9695	6.23×10^{-3}	1.74×10^{-1}	0.9997
	2.5	3.00×10^{-1}	1.16	2.72×10^{-1}	0.9368	1.38×10^{-2}	3.10×10^{-1}	0.9998
	5.0	3.66×10^{-1}	0.44	3.10×10^{-1}	0.8604	1.52×10^{-2}	3.77×10^{-1}	0.9930
	10.0	4.59×10^{-1}	0.49	3.86×10^{-1}	0.8468	2.92×10^{-2}	4.79×10^{-1}	0.9900
Pb(II)	0.1	1.74×10^{-2}	2.13	1.72×10^{-2}	0.9966	1.39×10^{-5}	1.77×10^{-2}	0.9995
	0.2	5.30×10^{-2}	2.38	4.94×10^{-2}	0.9892	2.00×10^{-4}	5.23×10^{-2}	0.9988
	0.3	6.45×10^{-2}	2.67	6.18×10^{-2}	0.9937	6.57×10^{-4}	6.42×10^{-2}	0.9993
	0.4	7.10×10^{-2}	3.56	6.92×10^{-2}	0.9978	1.11×10^{-3}	7.10×10^{-2}	0.9996
	0.5	9.40×10^{-2}	3.39	9.19×10^{-2}	0.9386	3.26×10^{-2}	9.56×10^{-2}	0.9997
	1.0	2.00×10^{-1}	3.07	2.02×10^{-1}	0.9967	3.61×10^{-2}	2.07×10^{-1}	0.9997
	2.5	3.89×10^{-1}	0.75	3.55×10^{-1}	0.9330	3.78×10^{-2}	3.97×10^{-1}	0.9997
	5.0	4.25×10^{-1}	0.87	3.96×10^{-1}	0.8562	4.00×10^{-2}	4.80×10^{-1}	0.9998
	10.0	5.30×10^{-1}	1.51	4.24×10^{-1}	0.8079	4.39×10^{-2}	5.51×10^{-1}	0.9996

Table 5.2 Langmuir and Freundlich isotherm parameters

Heavy metal ion	Temperature (^{o}C)	Langmuir isotherm			Freundlich isotherm		
		q_m (mmol g^{-1})	b (L mmol^{-1})	R^2	K_F	$1/n$	R^2
Cu(II)	25	0.45	0.19	0.9911	0.54	0.49	0.9485
	40	0.80	0.58	0.9675	0.07	0.22	0.8373
	60	0.85	1.21	0.9855	0.20	0.44	0.9623
Pb(II)	25	0.55	0.23	0.9969	0.31	0.39	0.7976
	40	0.85	1.87	0.9858	0.38	0.52	0.9413
	60	0.89	2.94	0.9877	0.46	0.46	0.8943

Table 5.3 Kinetic parameters of second-order models for the adsorption of Cu(II) and Pb(II) at various temperature

Metal	Temperature (^{0}C)	k_2 (g mmol^{-1} min^{-1})	$q_{e,cal}$ (mmol g^{-1})	R^2
Cu(II)	25	2.92×10^{-2}	4.39×10^{-2}	0.9900
	40	9.98×10^{-2}	7.33×10^{-1}	0.9912
	60	9.97×10^{-2}	8.34×10^{-1}	0.9976
Pb(II)	25	4.39×10^{-2}	5.51×10^{-1}	0.9847
	40	1.35×10^{-1}	8.52×10^{-1}	0.8364
	60	2.45×10^{-1}	9.08×10^{-1}	0.8423

Table 5.4 FT-IR results from metal laden activated carbon

| FT-IR peak | Frequency (cm^{-1}) | | | | | Assignment |
	Original activated acrbon (A)	Cu(II)-loaded activated carbon (B)	Differences (A-B)	Pb(II)-loaded activated carbon (C)	Differences (A-C)	
1	3,390.59	3,429.33	-38.74	3,404.93	-14.34	Bonded –OH groups
2	2,943.07	2,918.11	+24.96	2,920.20	+22.87	Aliphatic C–H group
3	2,866.90	*2,848.74	+18.16	**2,065.57	+801.33	*Aliphatic C–H group ** C=O stretching
4	1,693.14	1,698.60	-5.46	1,695.61	-2.47	C=O stretching
5	1,590.93	1,590.24	+0.69	1,584.62	+6.31	Secondary amine group
6	1,417.04	1,353.03	+64.01	1,355.30	+61.74	Symmetric bending of CH$_3$
7	1,200.85	1,230.37	-29.52	1,225.82	-24.97	C–O stretching
8	1,088.49	1,093.76	-5.27	1,050.54	+37.95	P-O
9	828.21	828.52	-0.31	824.86	+3.35	–CN stretching
10	516.88	-	-	573.75	-56.87	Alkane
11	500.36	533.14	-32.78	535.37	-35.01	Alkane

Table 5.5 Desorption of Cu(II) and Pb(II) (single component, solvent concentration = 1 N, T = 75^{0}C, and shaking rate = 200 rpm)

Desorbing agent	Extraction efficiency (%)							
	Cu				Pb			
	I[*]	II[*]	III[*]	Total	I[*]	II[*]	III[*]	Total
DI water	9.96	3.42	0.05	13.43	3.00	0.85	0.01	3.87
Phosphoric acid	58.03	4.87	0.12	63.02	15.52	1.23	0.03	16.78
Sulfuric acid	77.70	4.54	0.08	82.32	0.21	0.42	0.02	0.65
Citric acid	90.39	5.16	0.25	95.80	90.78	1.35	0.02	92.14

[*] Desorption sequence number: I = first, II = second and III = third desorption

Table 5.6 Extraction efficiency of Cu and Pb from Cu-Pb binary component (solvent concentration = 1 N, T = 75^{0}C and shaking rate = 200 rpm)

Desorbing agent	Extraction efficiency (%)								Cu(II) Extraction ratio
	Cu				Pb				
	I[*]	II[*]	III[*]	Total	I[*]	II[*]	III[*]	Total	
DI water	5.625	0.678	0.112	6.416	3.793	0.449	1.011	5.254	0.4846
Phosphoric acid	29.259	5.473	1.154	35.887	10.886	1.349	0.278	12.513	0.6883
Sulfuric acid	67.069	2.087	0.198	69.353	0.558	0.053	0.003	0.614	0.9888
Citric acid	32.214	2.474	0.306	34.995	16.318	1.316	0.227	17.861	0.6013

[*] Desorption sequence number: I = first, II = second and III = third desorption

Table 5.7 Desorption of single and binary component at various temperatures (shaking rate = 200 rpm)

Heavy metal	Temperature (°C)	$q_{e,Ext,exp}$ (mmol g^{-1})	Extraction efficiency (%)	Pseudo-first order			Pseudo-second order		
				$k_{d,1}$ (min^{-1})	$q_{e,Ext,cal}$ (mmol g^{-1})	R^2	$k_{d,2}$ (g mmol^{-1} min^{-1})	$q_{e,Ext,cal}$ (mmol g^{-1})	R^2
Cu(II)	25	5.51×10^{-2}	87.86	1.13	1.04×10^{-1}	0.9520	0.58	5.51×10^{-2}	0.9876
	50	4.43×10^{-2}	90.07	1.68	6.05×10^{-2}	0.9223	3.60	4.33×10^{-2}	0.9804
	75	1.34×10^{-2}	95.80	1.69	6.43×10^{-2}	0.7031	4.58	2.13×10^{-2}	0.9975
Pb(II)	25	1.26×10^{-1}	76.62	0.92	1.79×10^{-1}	0.8625	0.33	1.29×10^{-1}	0.9849
	50	9.83×10^{-2}	81.81	1.26	1.49×10^{-1}	0.8216	2.63	9.97×10^{-2}	0.9926
	75	3.70×10^{-2}	92.14	1.31	1.37×10^{-1}	0.9450	3.69	2.37×10^{-2}	0.9929
Cu (Cu-Pb)	25	1.46×10^{-3}	59.03	2.12	1.32×10^{-3}	0.7498	1.31	1.44×10^{-3}	0.9972
	50	1.23×10^{-3}	65.89	1.76	2.65×10^{-2}	0.9855	3.24	1.20×10^{-3}	0.9981
	75	1.10×10^{-3}	69.35	2.07	1.68×10^{-3}	0.9576	15.09	1.09×10^{-3}	0.9988

Table 5.8 FT-IR results from original activated carbon, Cu(II)-adsorption and Cu(II)-desorption

| FT-IR peak | Frequency (cm^{-1}) | | | | Assigment |
	Original activated carbon (A)	Cu(II)-adsorption (B)	Cu(II)-desorption (C)	Differences (B-C)	
1	3390.59	3429.33	3433.66	-4.33	Bonded –OH groups
2	2943.07	2918.11	-	-	Aliphatic C–H group
3	2866.90	2848.74	-	-	Aliphatic C–H group,
4	1693.14	1698.60	1707.48	-8.88	C=O stretching
5	1590.93	1590.24	1601.82	-11.58	Secondary amine group
6	1417.04	1353.03	-	-	Symmetric bending of CH3
7	1200.85	1230.37	1184.55	45.82	C–O stretching
8	1088.49	1093.76	-	-	P-O
9	-	-	894.35	-	C–H group
10	828.21	828.52	-	-	–CN stretching
11	-	-	798.55	-	–CN stretching
12	-	-	588.67	-	Alkane
13	517.88	533.14	-	-	Alkane
14	500.36	-	-	-	Alkane

Table 5.9 FT-IR results from original activated carbon, Pb(II)-adsorption and Pb(II)-desorption

| FT-IR peak | Frequency (cm^{-1}) | | | | Assigment |
	Original activated carbon (A)	Pb(II)-adsorption (B)	Pb(II)-desorption (C)	Differences (B-C)	
1	3390.59	3404.93	3429.48	-24.55	Bonded –OH groups
2	2943.07	2920.20	-	-	Aliphatic C–H group
3	2866.90	-	-	-	Aliphatic C–H group,
4	-	2065.57	1807.87	257.70	C=O stretching
5	1693.14	1695.61	1706.16	-10.55	C=O stretching
6	1590.93	1584.62	1583.42	1.20	Secondary amine group
7	1417.04	1355.30	-	-	Symmetric bending of CH3
8	1200.85	1225.82	1188.29	37.53	C–O stretching
9	1088.49	1050.54	1053.21	-2.67	P-O
10	-	982.62	984.29	-	–CN stretching
11	-	-	897.08	-	–CN stretching
12	828.21	824.86	825.44	-0.58	–CN stretching
13	-	573.75	575.16	-1.41	Alkane
14	-	535.37	535.93	-0.56	Alkane
15	517.88	533.14	-	-	Alkane
16	500.36	-	-	-	Alkane

Table 5.10 FT-IR results from original activated carbon, binary-adsorption and binary-desorption

| FT-IR peak | Frequency (cm⁻¹) | | | | Assigment |
	Original activated carbon (A)	Binary-adsorption (B)	Binary-desorption (C)	Differences (B-C)	
1	3390.59	3412.22	3427.89	-15.67	Bonded –OH groups
2	2943.07	2920.58	-	-	Aliphatic C–H group
3	2866.90	-	-	-	Aliphatic C–H group,
4	1693.14	1698.96	1697.19	1.77	C=O stretching
5	1590.93	1589.55	1593.86	-4.31	Secondary amine group
6	1417.04	-	-	-	Symmetric bending of CH_3
7	-	1383.71	-	-	Symmetric bending of CH_4
8	1200.85	1226.47	1172.16	54.31	C–O stretching
9	1088.49	1085.82	1080.74	5.08	P-O
10	-	-	1051.82	-	P-O
11	-	-	968.43	-	–CN stretching
12	-	-	882.72	-	–CN stretching
13	828.21	828.69	779.98	48.71	–CN stretching
14	-	-	631.04	-	Alkane
15	-	574.08	594.78	-20.70	Alkane
16	517.88	536.45	-	-	Alkane
17	500.36	-	-	-	Alkane

Table 5.11 Cu(II) and Pb(II) adsorption capacities of various agricultural-based adsorbents

Adsorbent	Activation method	Surface area $(m^2\ g^{-1})$	Adsorption capacity $(mmol\ g^{-1})$		Ref.
			Cu (II)	Pb (II)	
Cloth-activated carbon	Physical	1,680	0.17	0.15	Faur-Brasquet et al., 2002
Activated carbon pretreated with citric acid	Chemical	431	0.23	-	Chen et al., 2003
Rice hull-activated carbon	Chemical	-	0.14	-	Ong et al., 2003
Coconut-activated carbon	Chemical	266	0.42	-	Sekar et al., 2004
Rubber wood sawdust-activated carbon	Chemical	1,674	0.09	-	Kalavathy et al., 2005
Apricot stone-activated carbon	Chemical	566	0.38	0.11	Kobya et al., 2005
Coconut-granular activated carbon	-	1,000	-	0.11	Goel et al., 2005
Coal-activated carbon	-	1,200	-	0.15	Machida et al., 2005
Ceiba pentandra hull-activated carbon	Physical	521	0.33	-	Rao et al., 2006
Peanut shell-activated carbon	Physical	725	0.84	0.74	Wilson et al., 2006
Eucalyptus bark-activated carbon	Chemical	1,239	0.45	0.55	This work
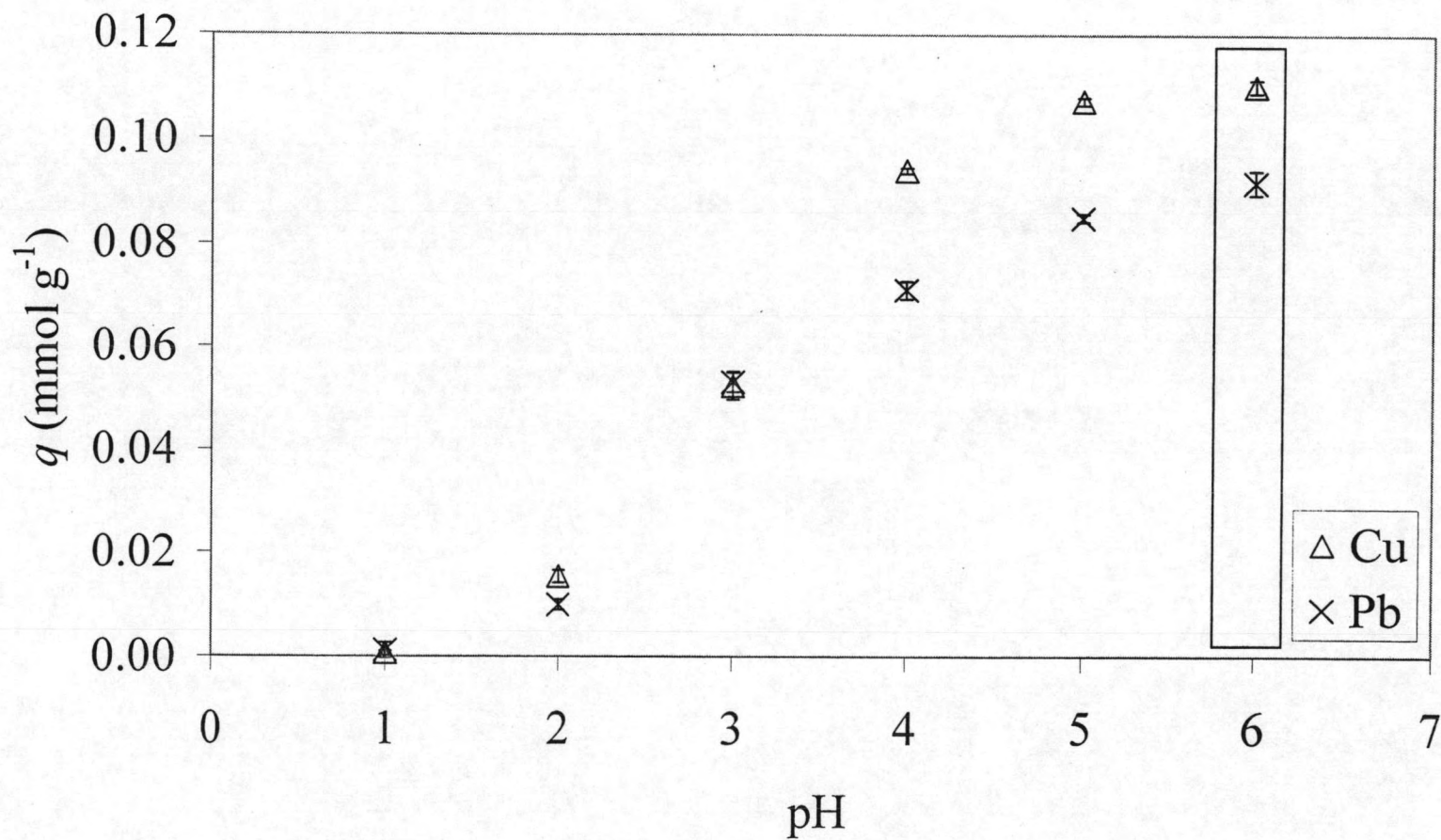
Figure 5.1 Effect of pH for adsorption (Initial concentration = 0.3 mmol L^{-1}, shaking rate = 200 rpm, 25°C)
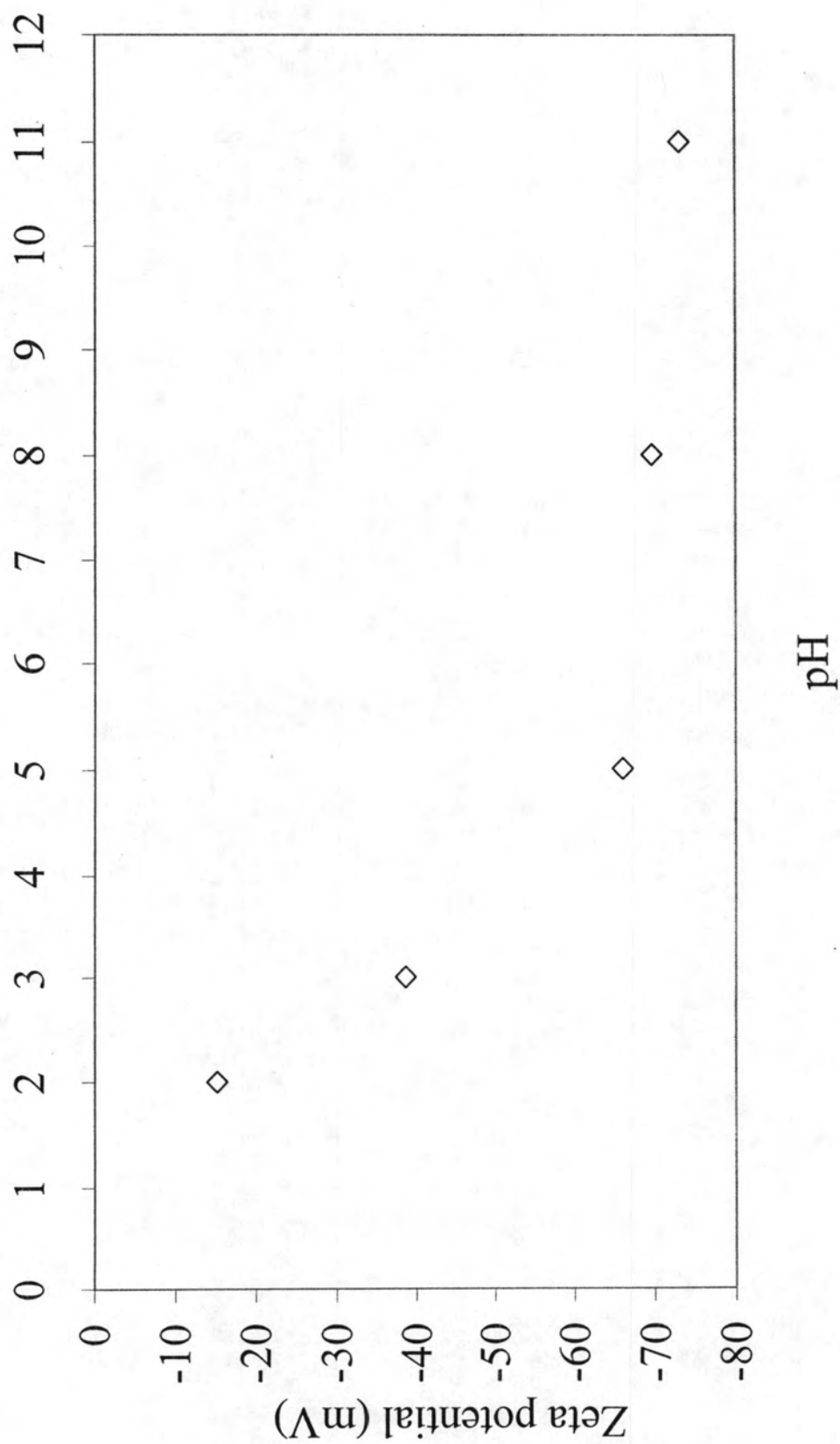
Figure 5.2 Relationship between surface charge of activated carbon and pH
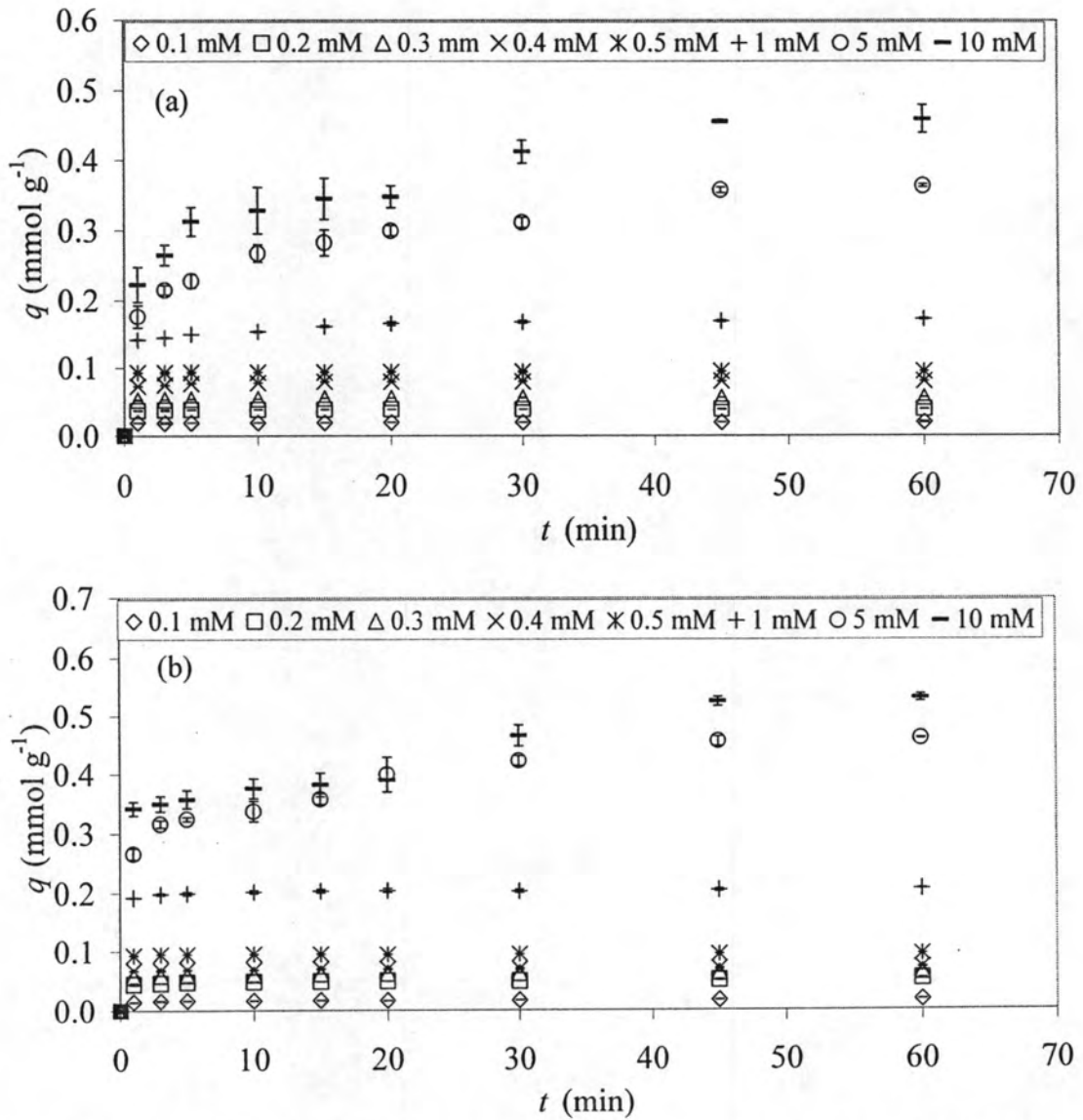
Figure 5.3 Adsorption kinetics (shaking rate = 200 rpm, 25°C, pH =5) (a) Cu(II) (b) Pb(II)
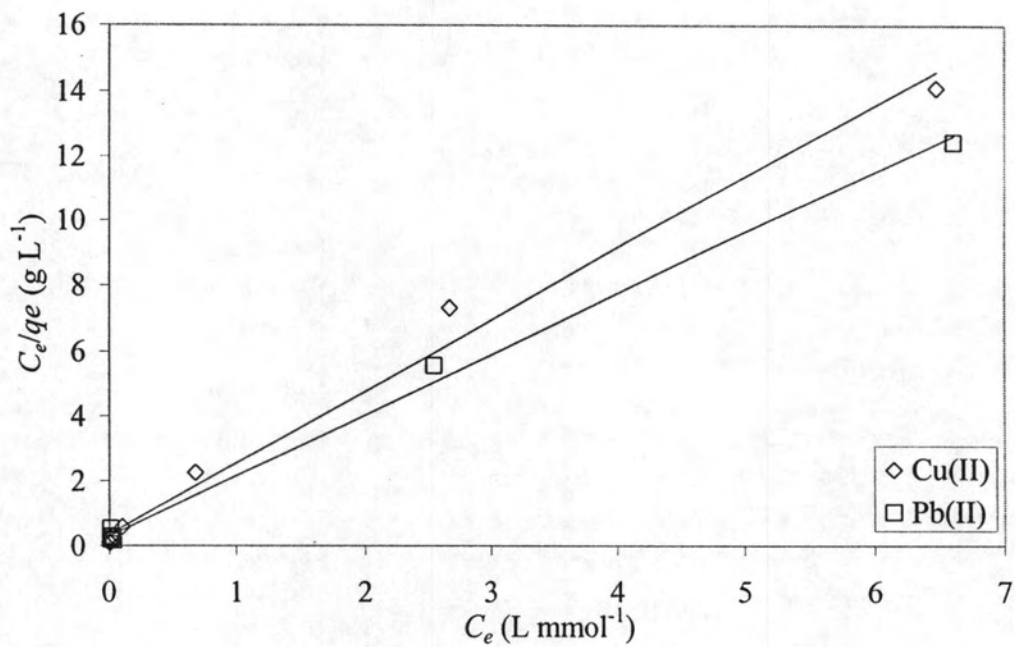
Figure 5.4 Langmuir isotherm plots for the adsorption of Cu(II) and Pb(II) onto activated carbon (shaking rate = 200 rpm, 25°C, pH =5)
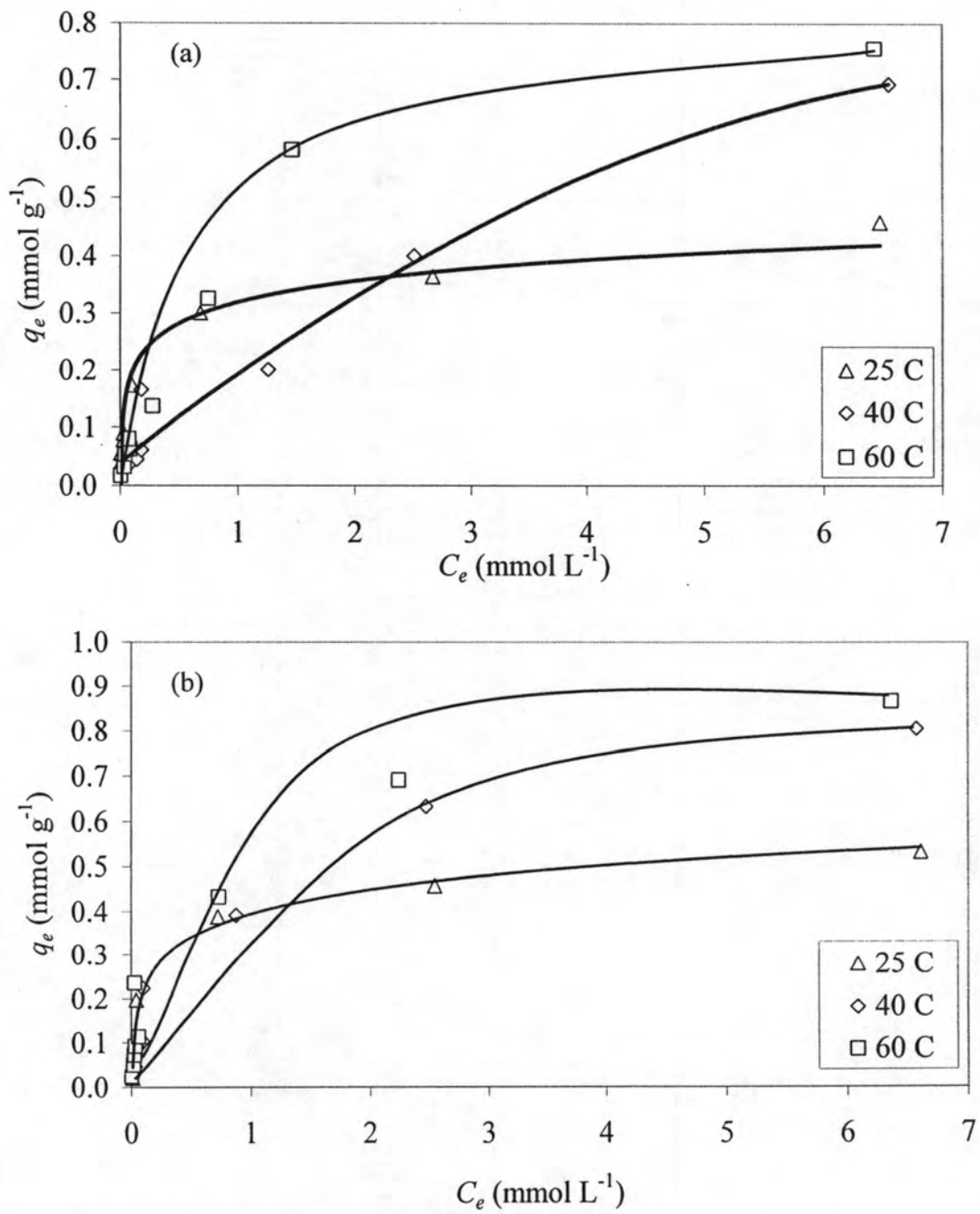
Figure 5.5 Adsorption isotherm (a) Cu(II) (b) Pb(II)
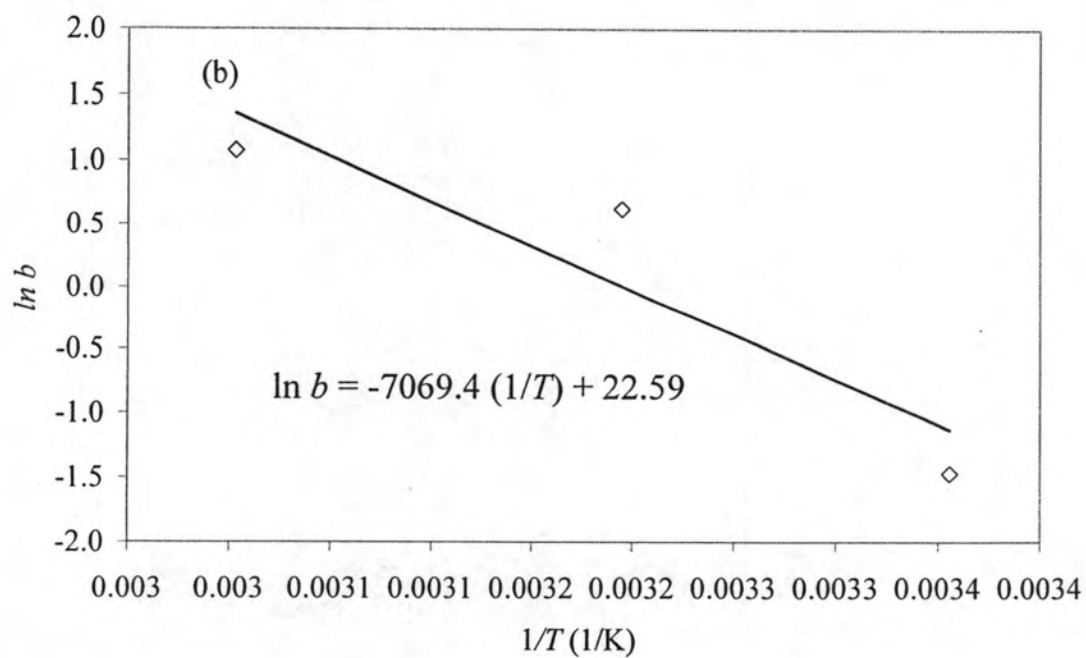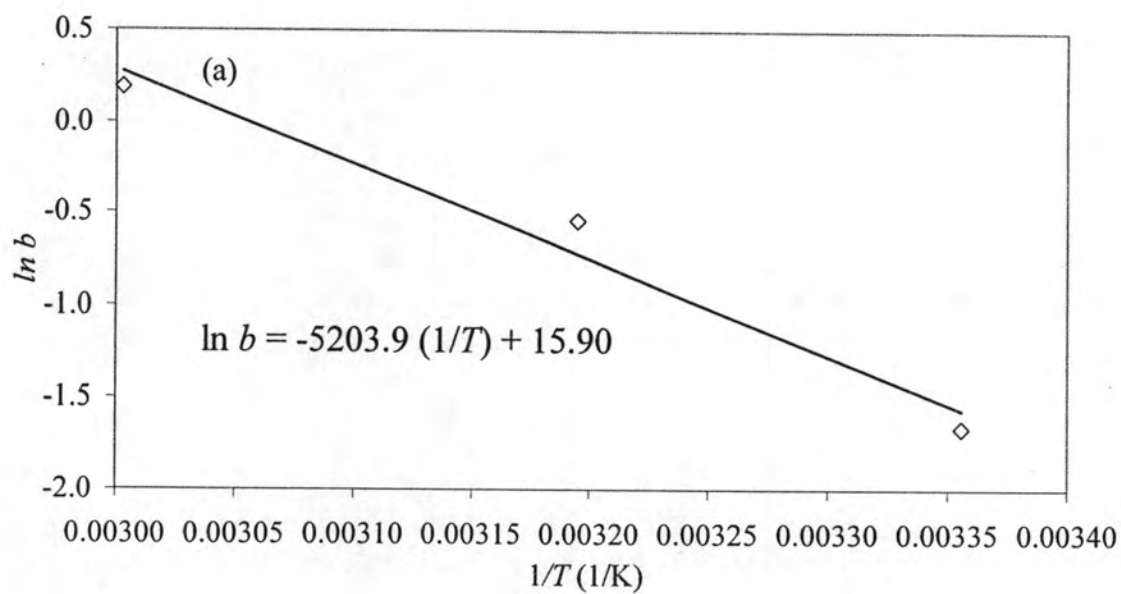
Figure 5.6 Plot of ln b versus 1/T for (a) Cu(II) (b) Pb(II) for the determination of adsorption enthalpy
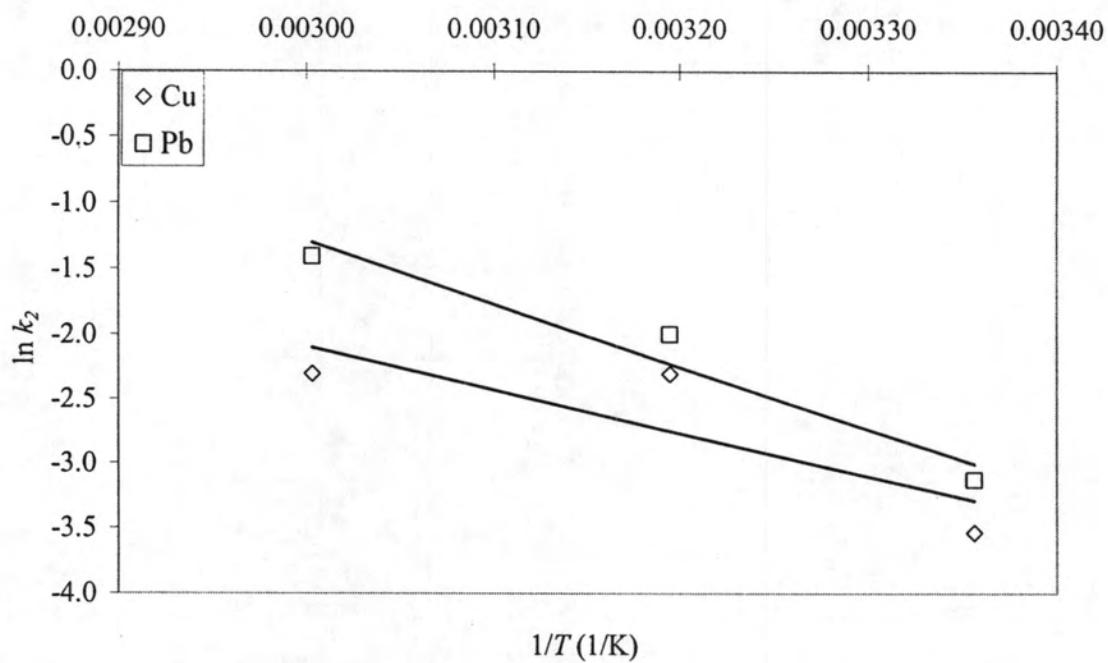
Figure 5.7 Plots ln k_2 vs. $1/T$ of (a) Cu(II) (b) Pb(II) for the determination of activation energy for adsorption
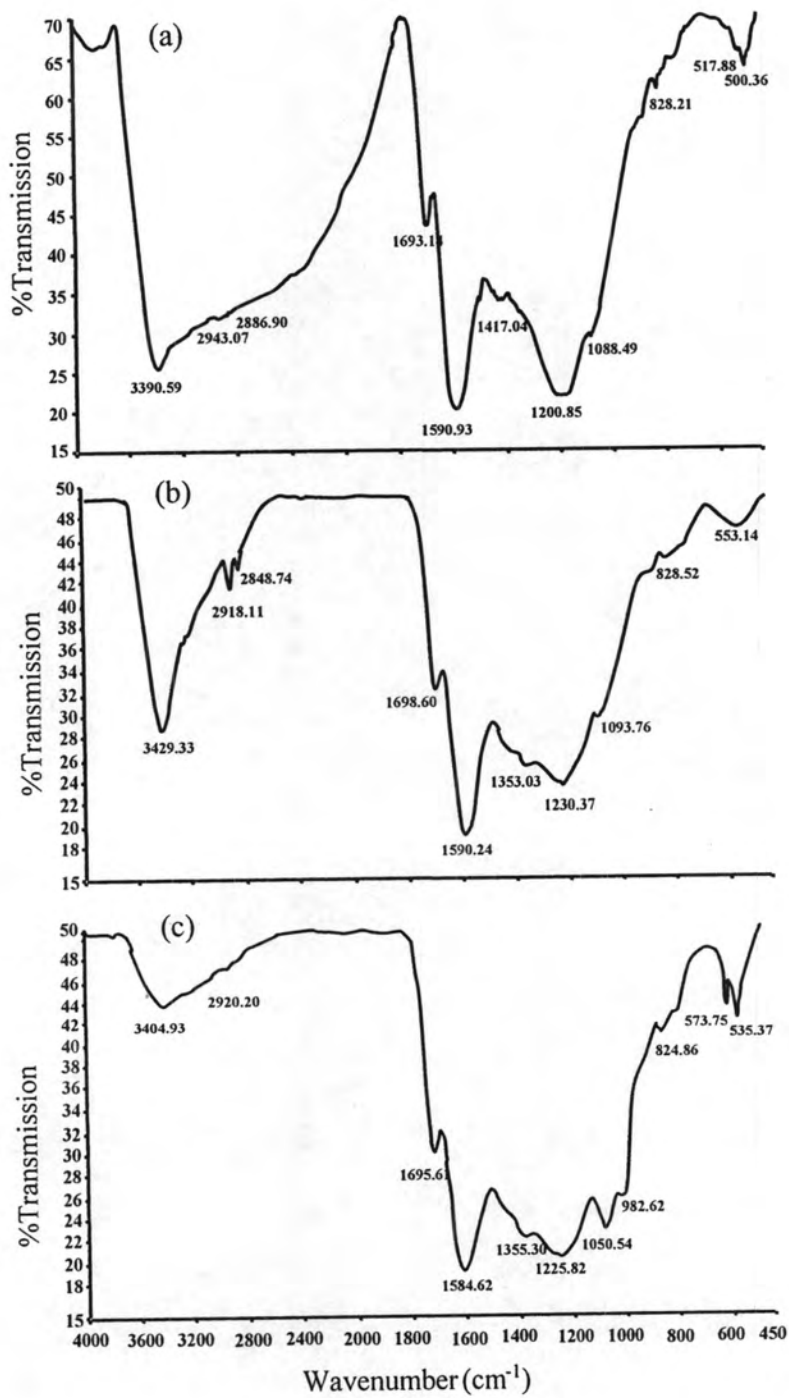
Figure 5.8 FT-IR transmission spectra (a) original activated carbon (b) Cu(II) laden activated carbon (c) Pb(II) laden activated carbon
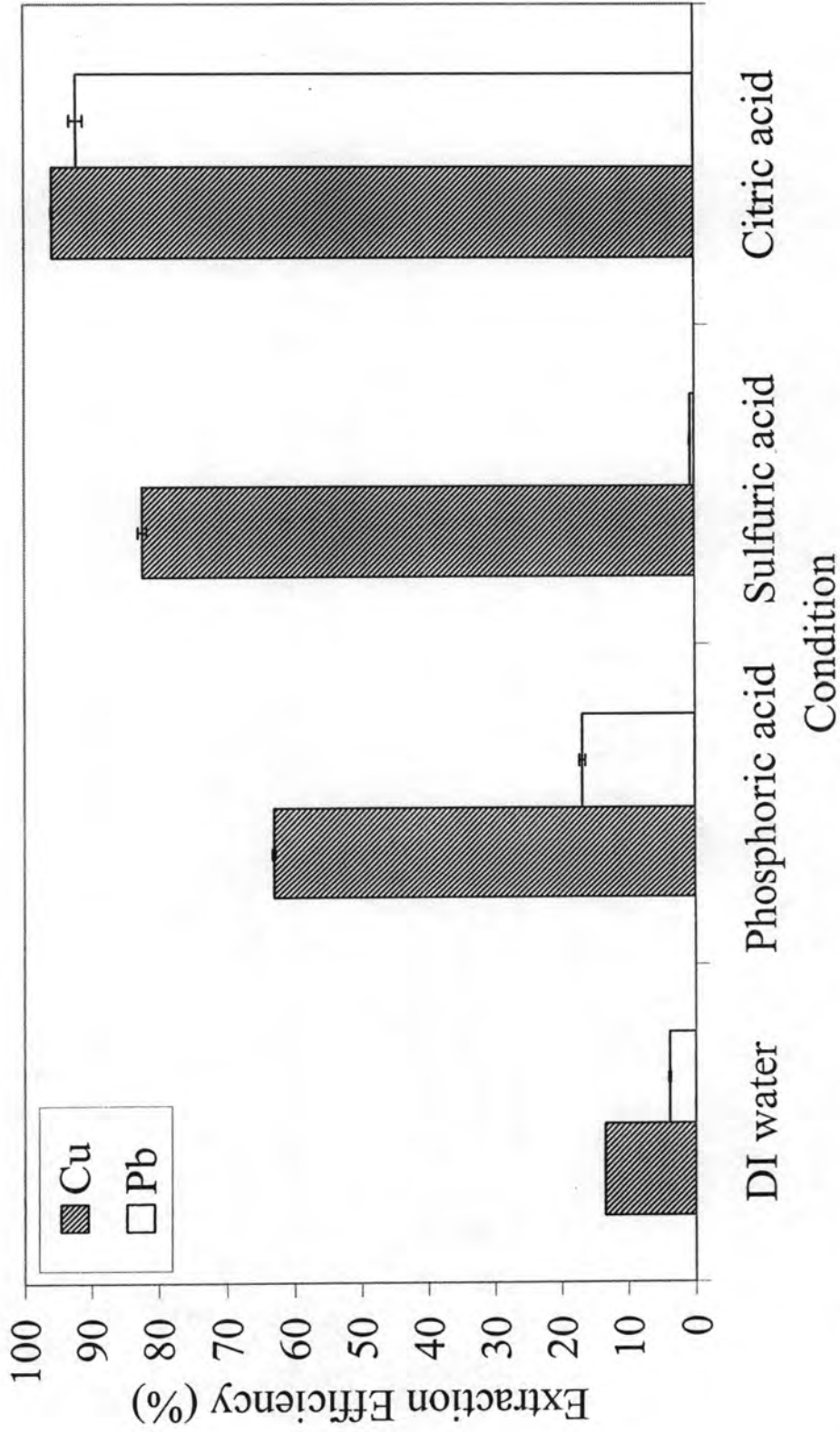
Figure 5.9 Effect of the type of solvent for desorption Cu(II) and Pb(II) (single component, solvent concentration = 1 N, T= 75 °C and shaking rate = 200 rpm)
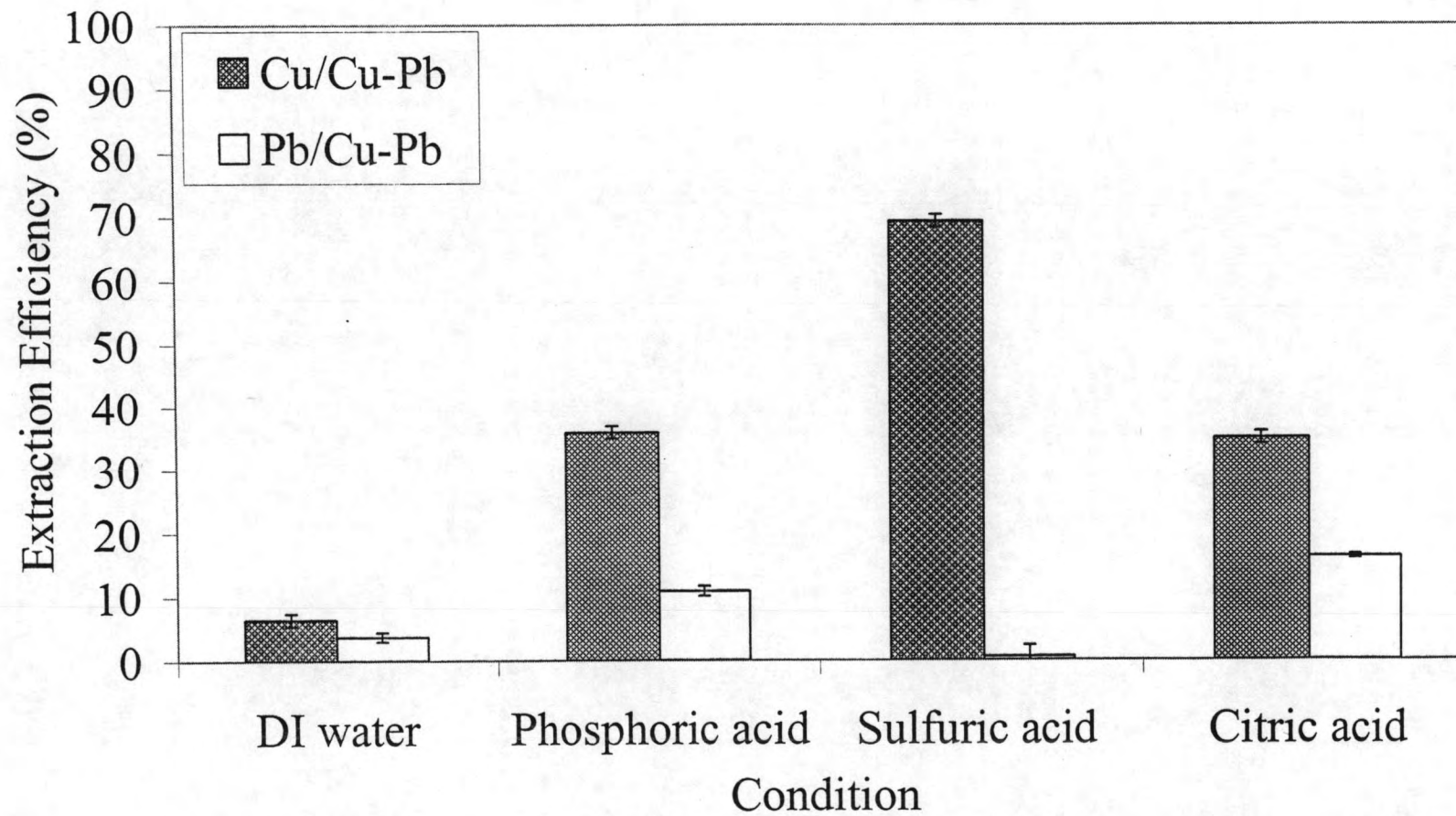
Figure 5.10 Effect of the type of solvent for desorption Cu(Cu-Pb) and Pb(Cu-Pb) (binary component, solvent concentration = 1 N, T= 75 ^{0}C and shaking rate = 200 rpm)
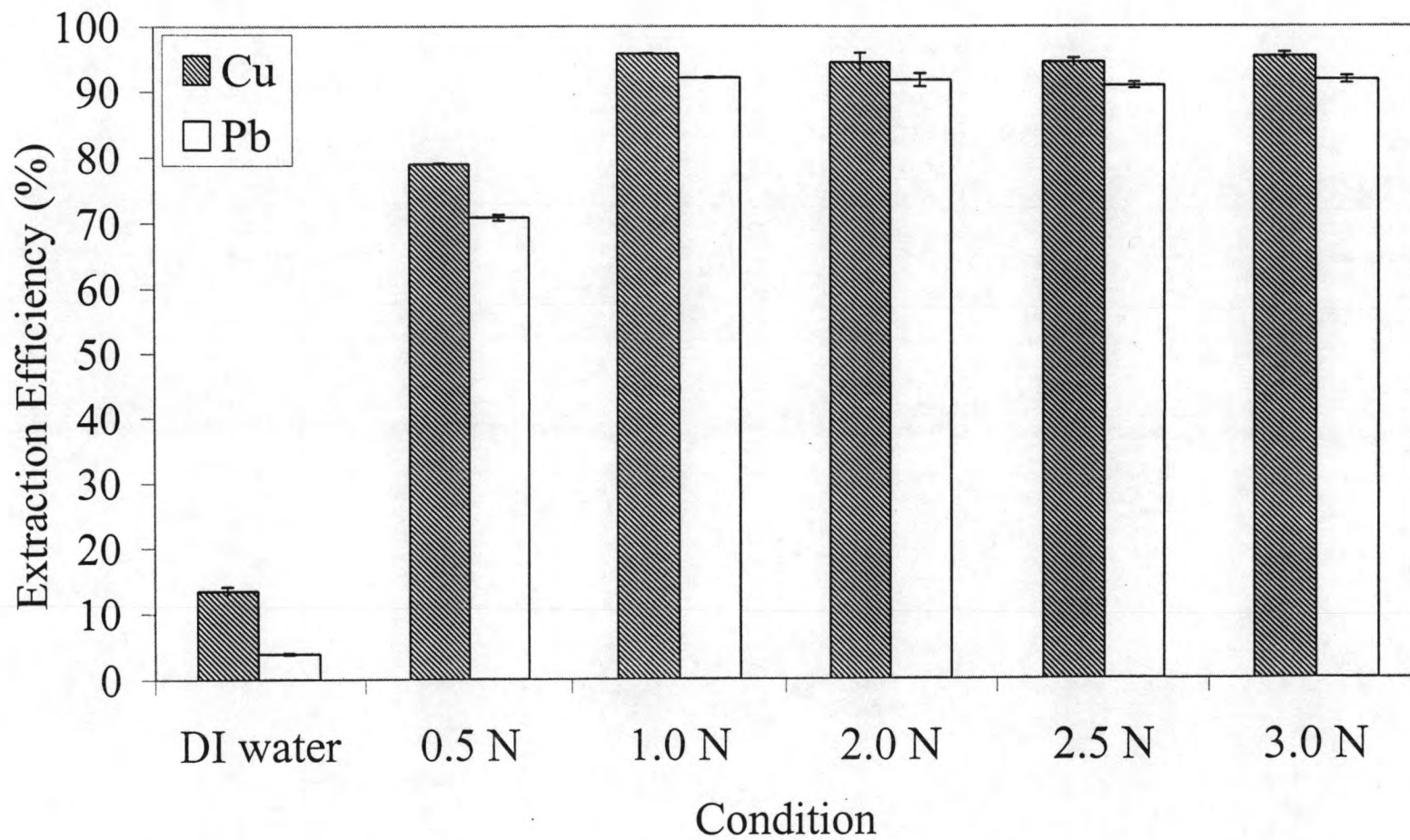
Figure 5.11 Effect of solvent concentration for desorption Cu(II) and Pb(II) at various concentration (single component, citric acid, 75°C and shaking rate = 200 rpm)
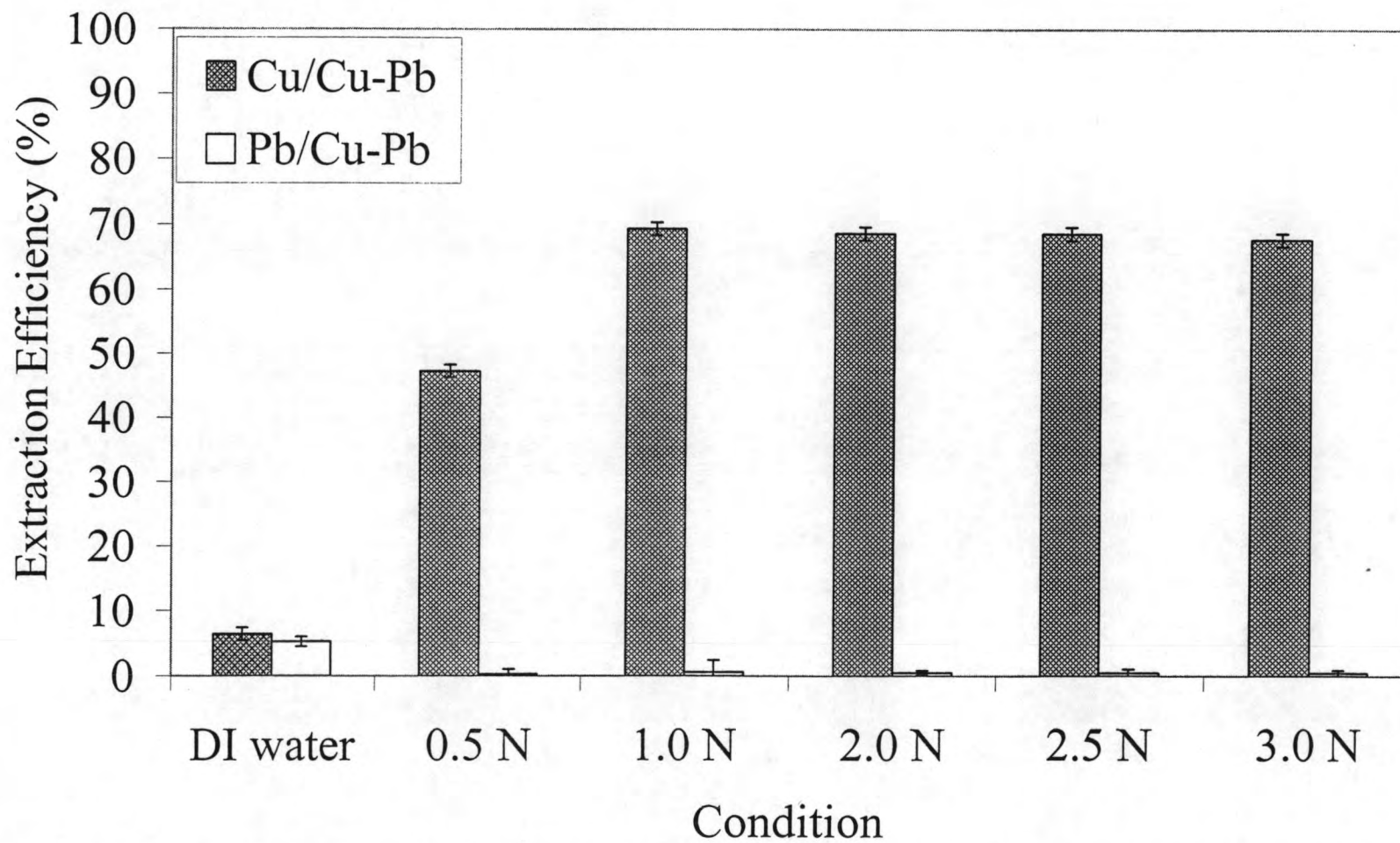
Figure 5.12 Effect of solvent concentration for desorption Cu(Cu-Pb) and Pb(Cu-Pb) at various concentration (binary component, citric acid, 75°C and shaking rate = 200 rpm)
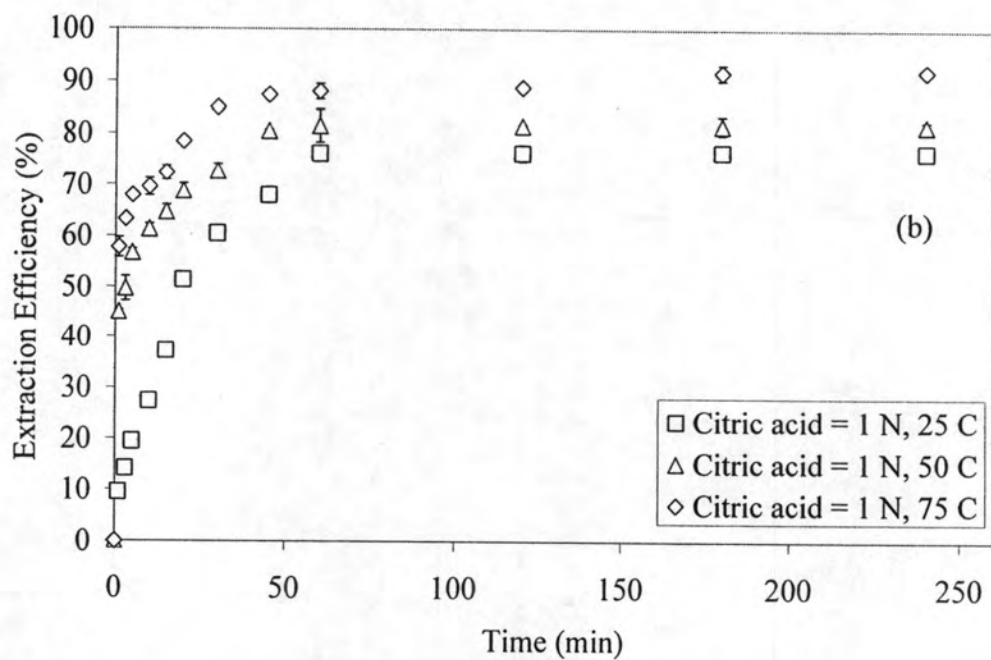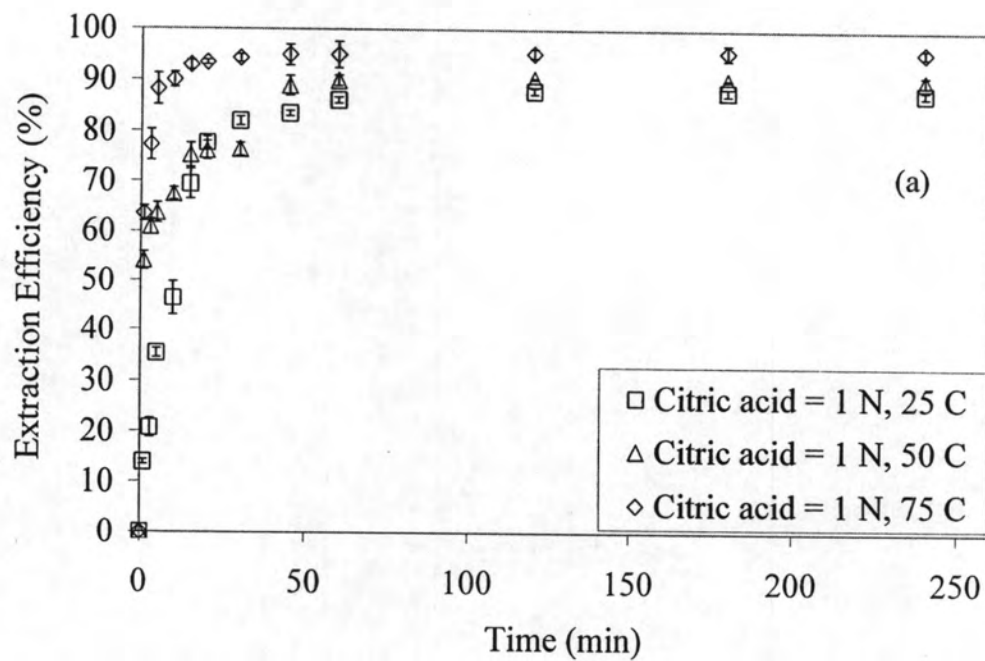
Figure 5.13 Effect of temperature for desorption (a) Cu(II) and (b) Pb(II) (single component, 1 N citric acid, shaking rate = 200 rpm)
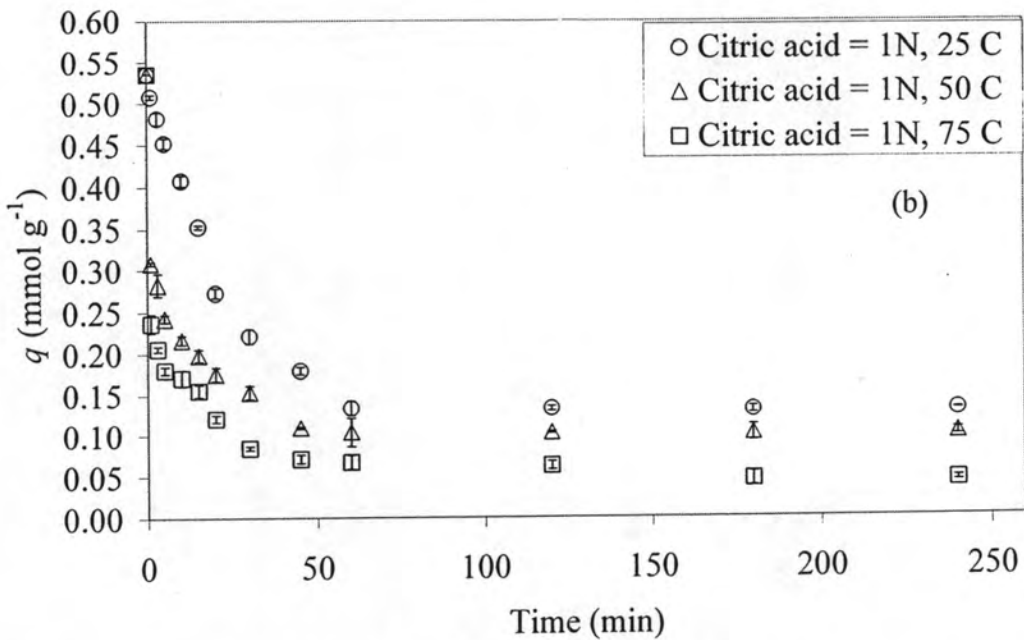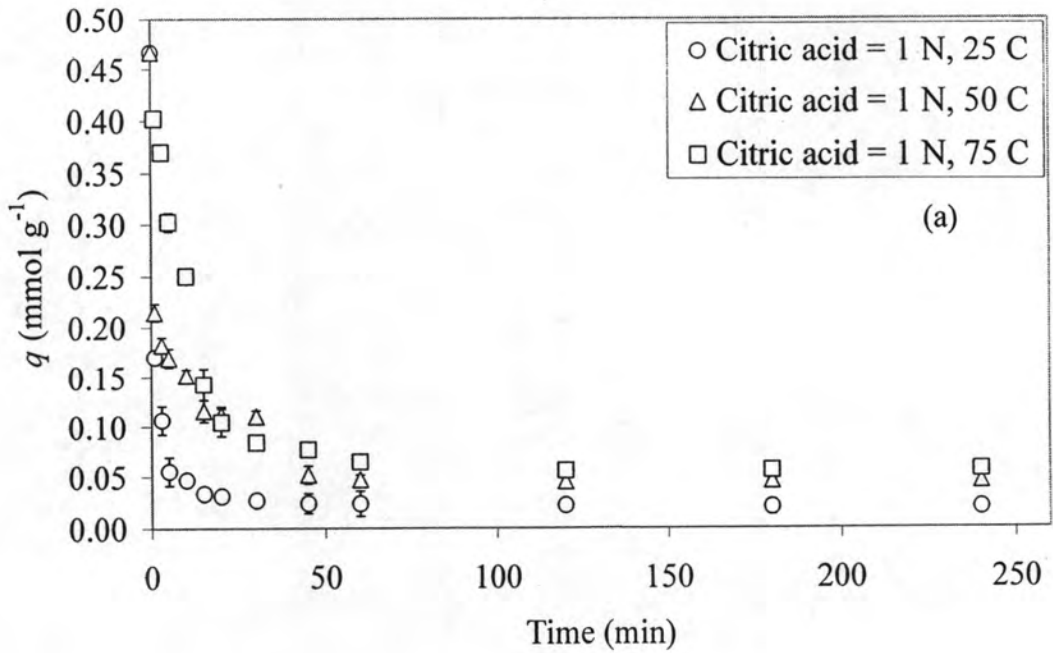
Figure 5.14 Extraction kinetics of (a) Cu(II) and (b) Pb(II)) (single component, 1 N citric acid, shaking rate = 200 rpm)
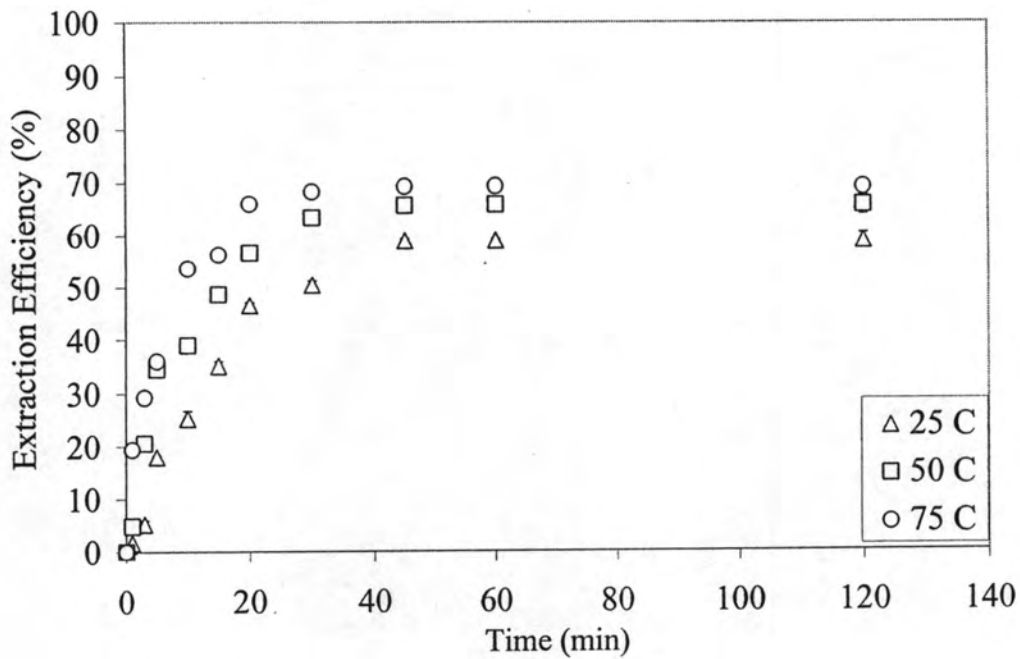
Figure 5.15 Effect of temperature for desorption Cu(Cu-Pb) (binary component, 1 N citric acid, shaking rate = 200 rpm)
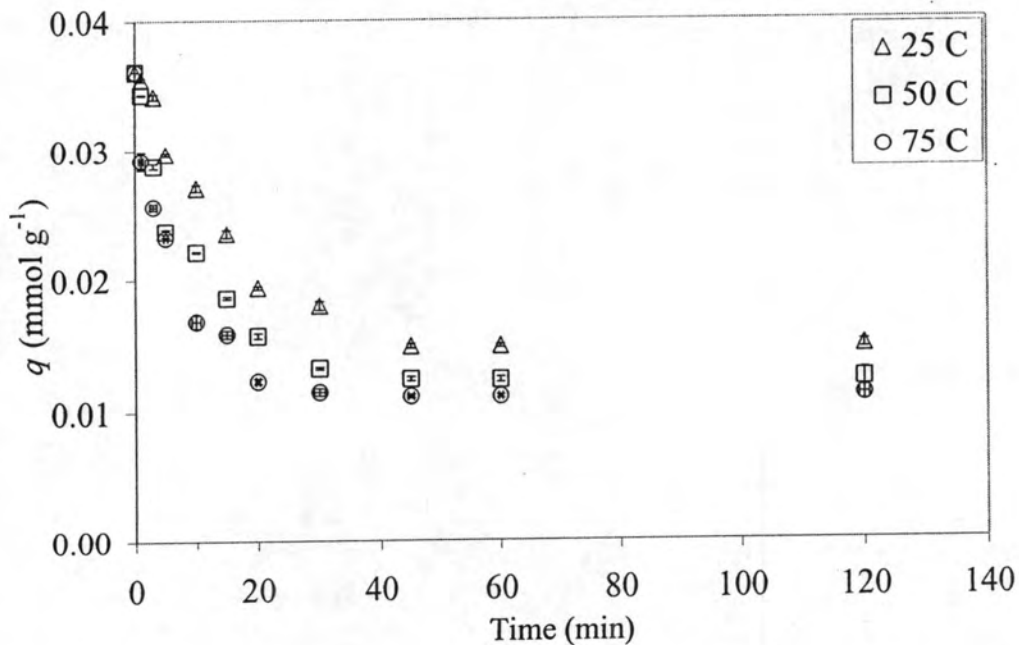
Figure 5.16 Extraction kinetics of Cu(Cu-Pb) (binary component, 1 N citric acid, shaking rate = 200 rpm)
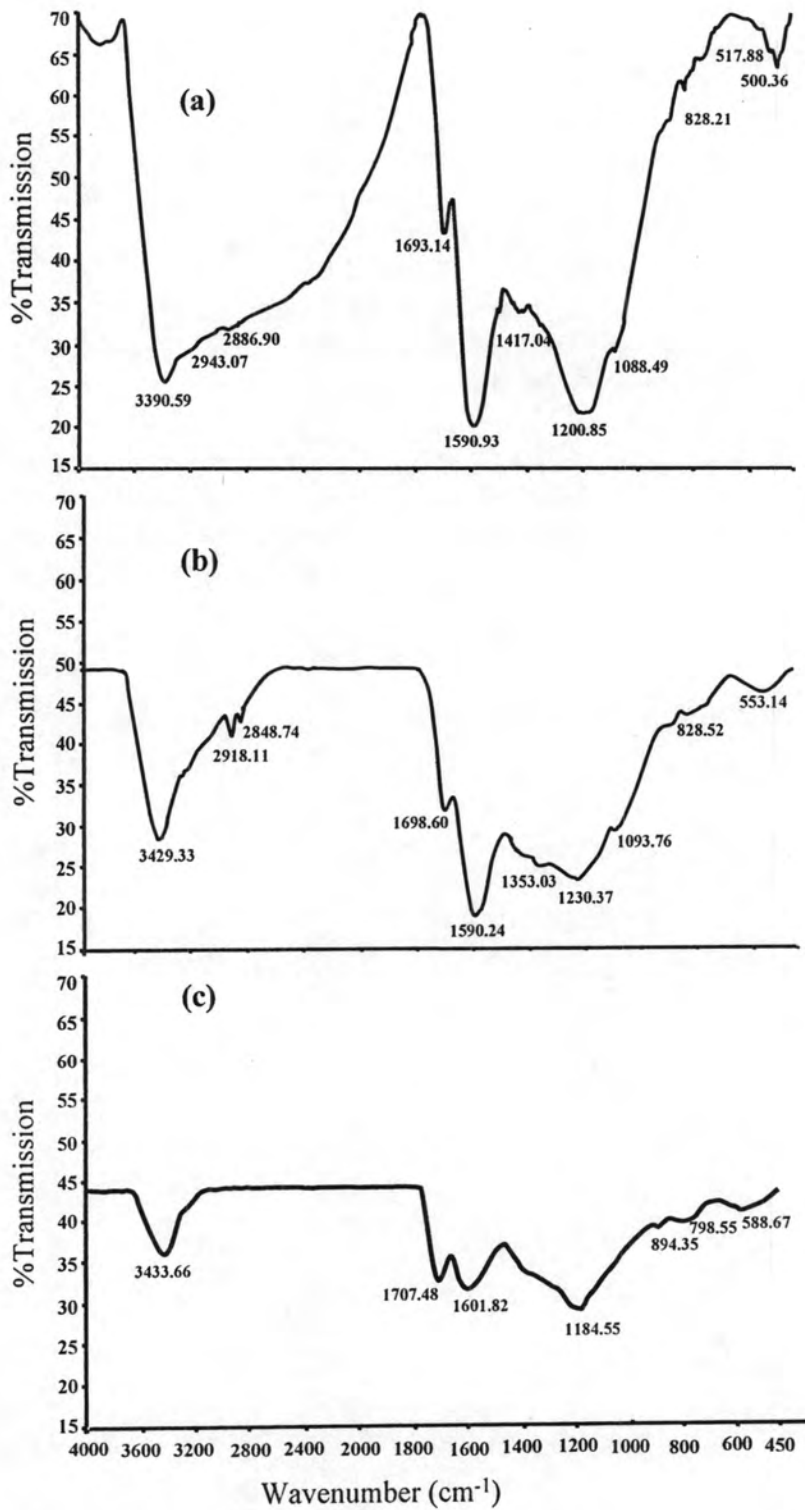
Figure 5.17 FT-IR transmission spectra (a) Original activated carbon (b) Cu-adsorption (c) Cu-desorption
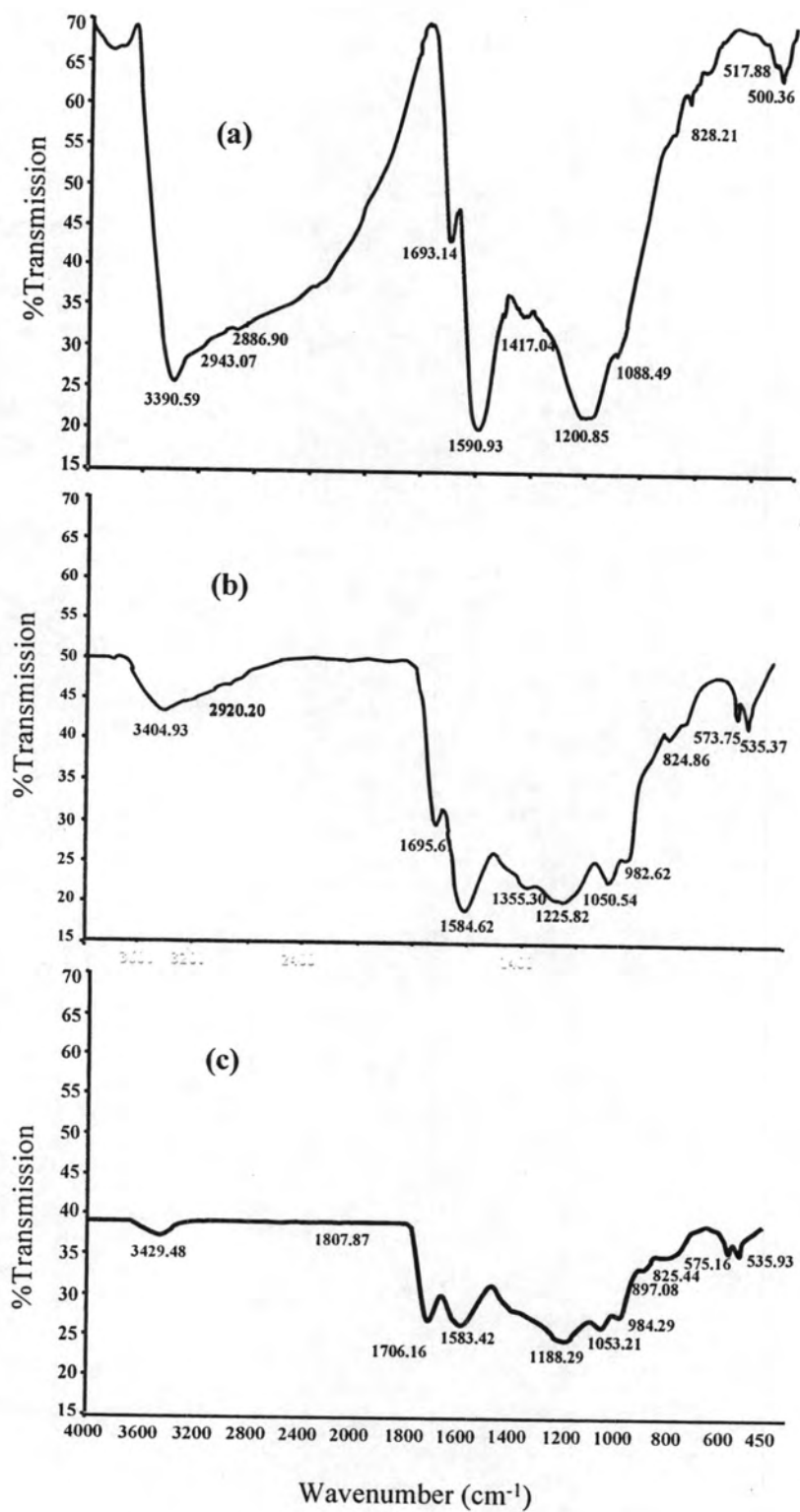
Figure 5.18 FT-IR transmission spectra (a) Original activated carbon (b) Pb-adsorption
(c) Pb-desorption
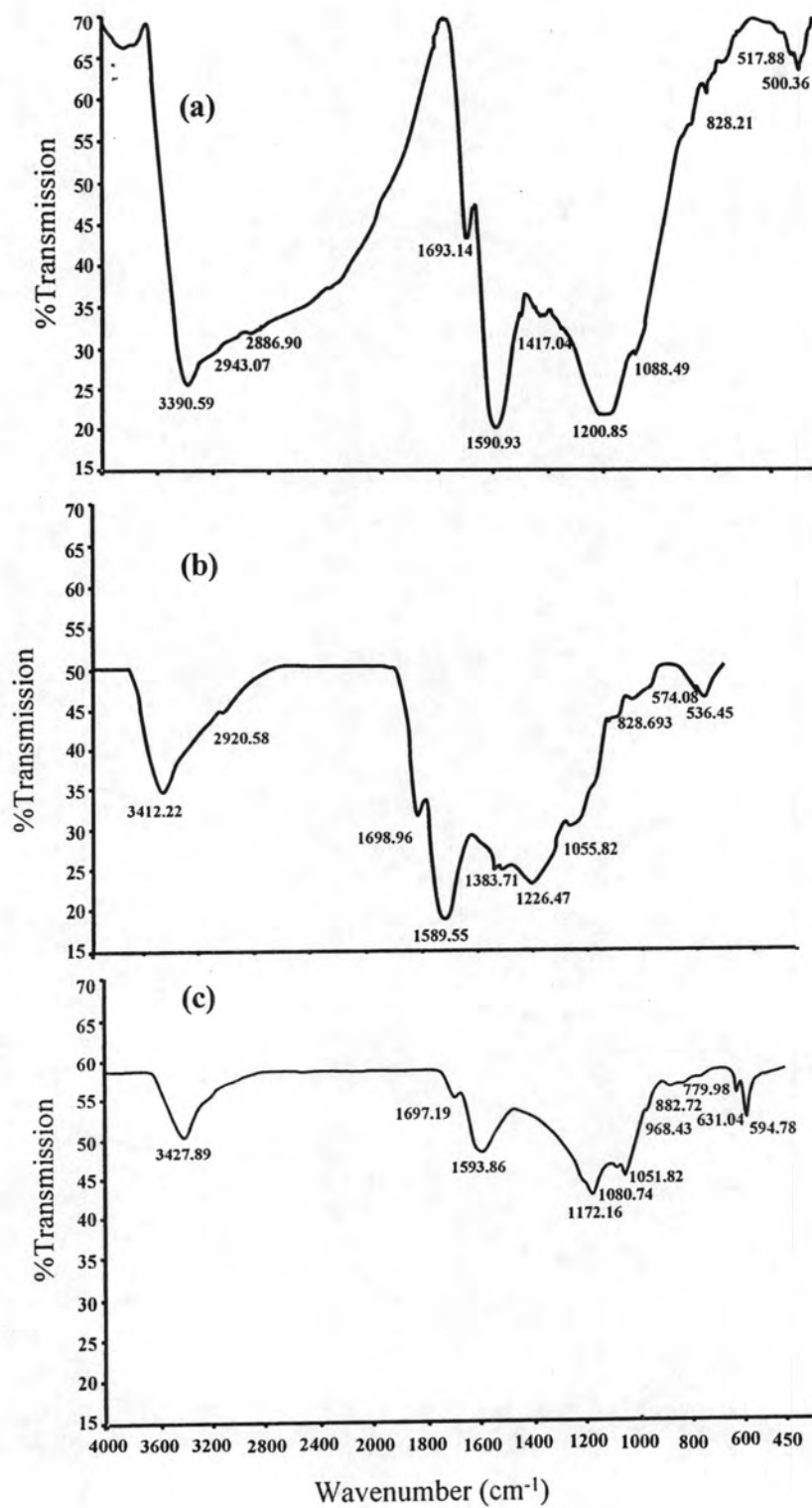
Figure 5.19 FT-IR transmission spectra (a) Original activated carbon (b) Binary-adsorption (c) Binary-desorption
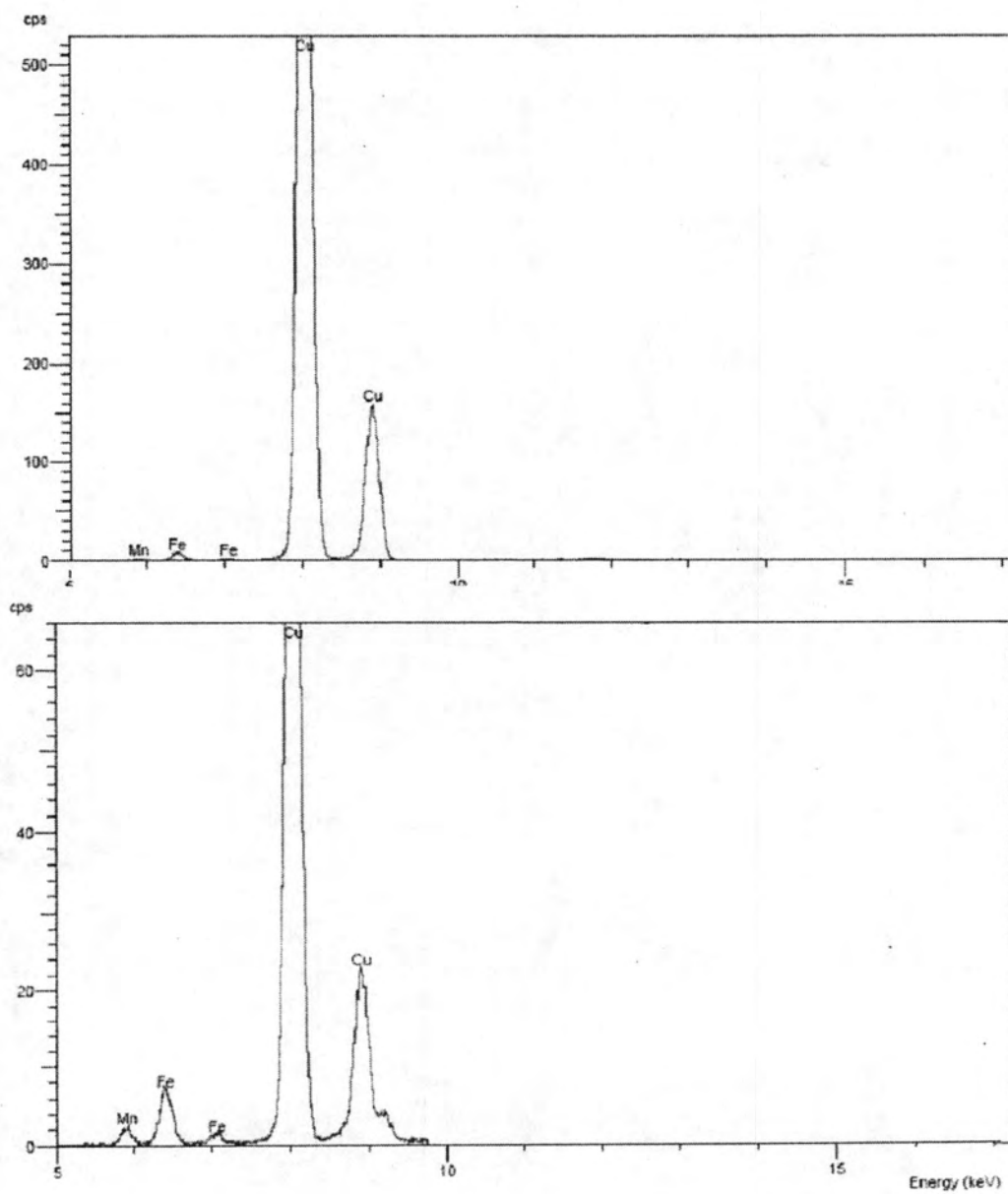
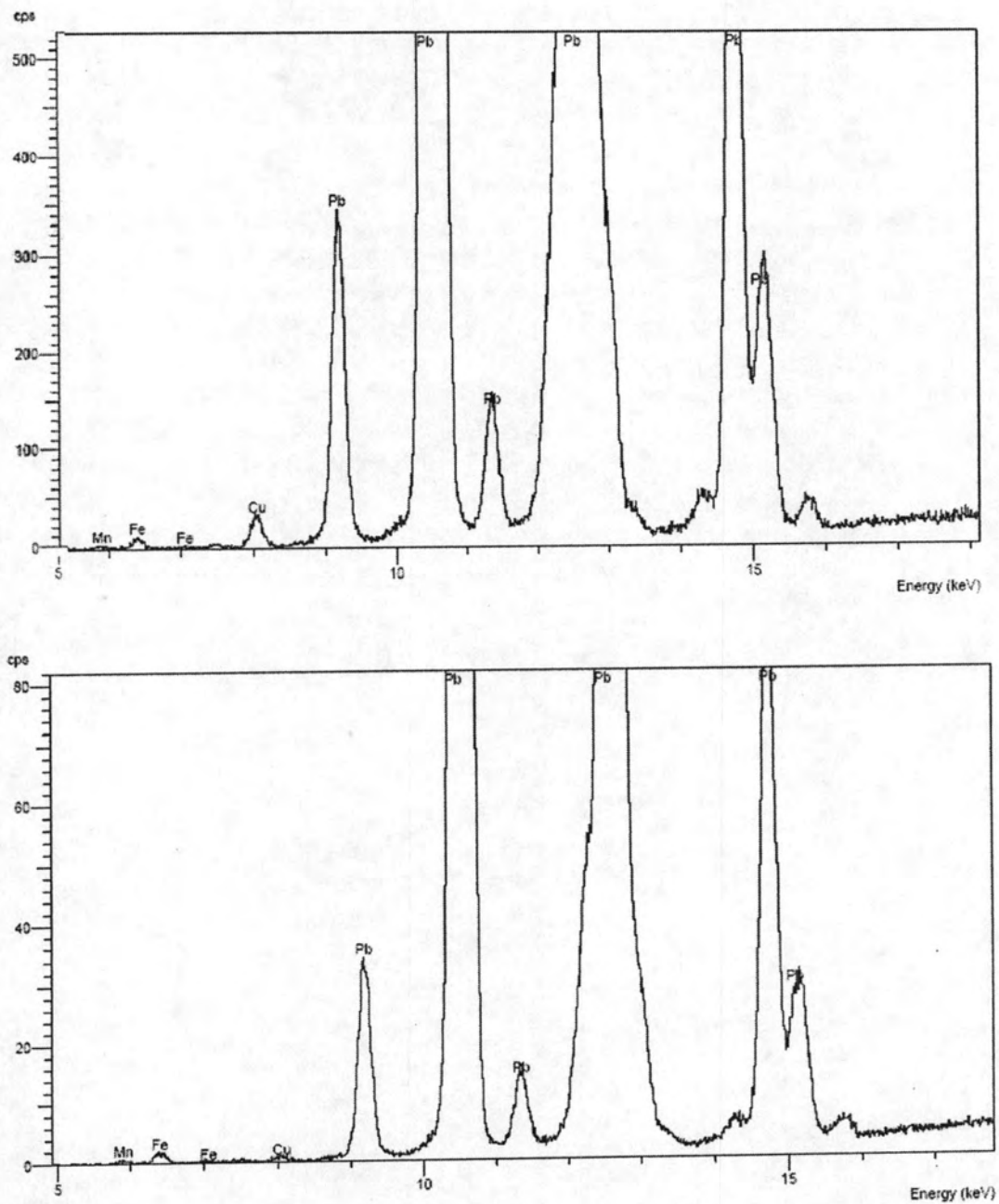Figure 5.20 XRF patterns for (a) Cu-adsorption (b) Cu-desorption

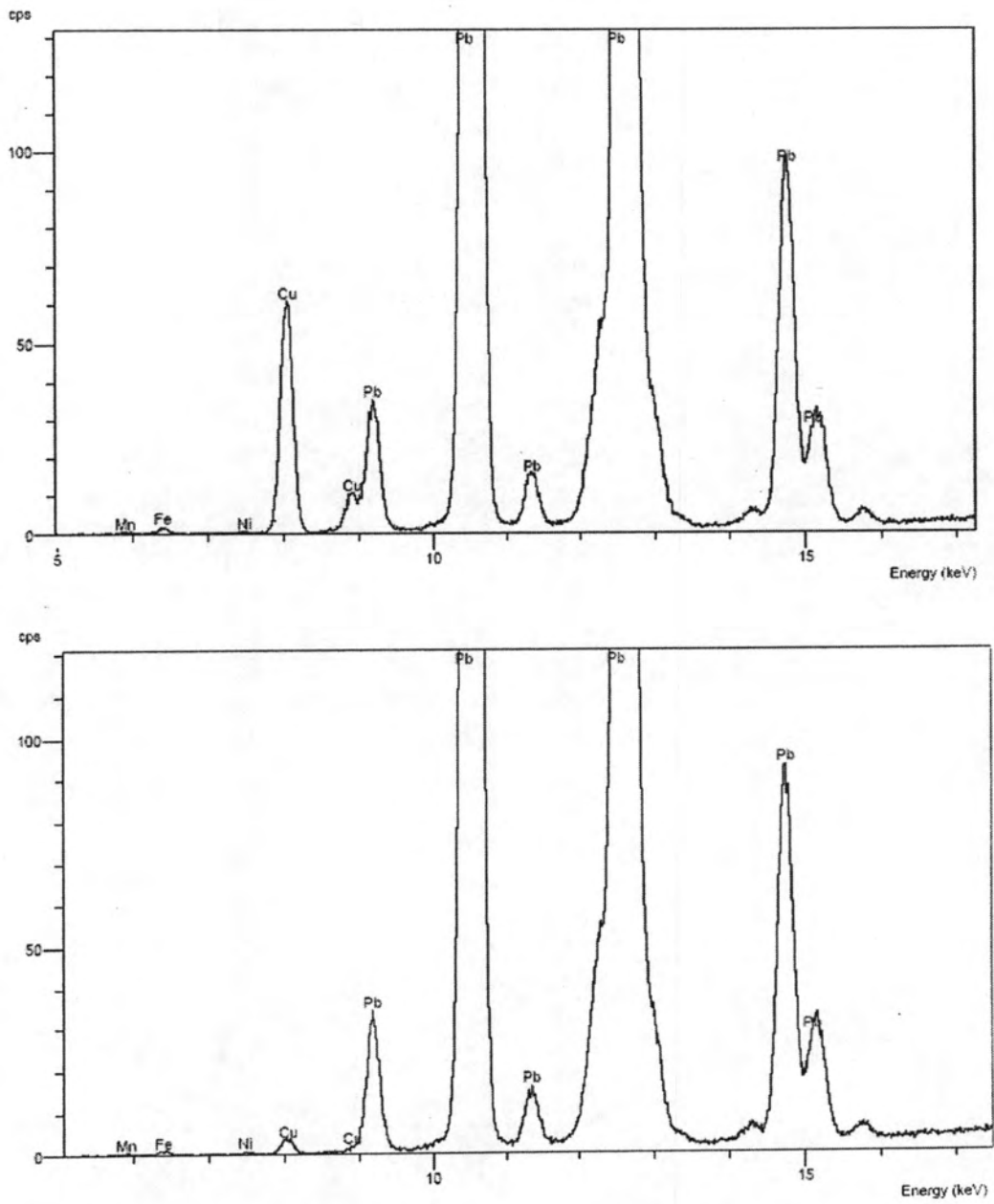Figure 5.21 XRF patterns for (a) Pb-adsorption (b) Pb-desorption

Figure 5.22 XRF patterns for (a) Binary-adsorption (b) Binary-desorption